Lithos 168–169 (2013) 85–98

Contents lists available at SciVerse ScienceDirect

Lithos

journal homepage: www.elsevier.com/locate/lithos

Ca. 1.5 Ga mafic magmatism in South China during the break-up of the supercontinent Nuna/Columbia: The Zhuqing Fe–Ti–V oxide ore-bearing mafic intrusions in western Yangtze Block

Hong-Peng Fan [a,c], Wei-Guang Zhu [a,*], Zheng-Xiang Li [b], Hong Zhong [a], Zhong-Jie Bai [a], De-Feng He [a], Cai-Jie Chen [d], Chong-Yong Cao [d]

[a] State Key Laboratory of Ore Deposit Geochemistry, Institute of Geochemistry, Chinese Academy of Sciences, 46 Guanshui Road, Guiyang 550002, China
[b] ARC Center of Excellence for Core to Crust Fluid Systems (CCFS) and The Institute for Geoscience Research (TIGeR), Department of Applied Geology, Curtin University, GPO Box U1987, Perth, Western Australia 6845, Australia
[c] University of Chinese Academy of Sciences, Beijing 100049, China
[d] Geological Team 601, Sichuan Bureau of Metallurgical Geology and Mineral Exploration, Panzhihua 617027, China

ARTICLE INFO

Article history:
Received 21 August 2012
Accepted 8 February 2013
Available online 16 February 2013

Keywords:
Mesoproterozoic
Mafic intrusion
Zircon and baddeleyite geochronology
Yangtze Block
Supercontinent Nuna/Columbia
Fe–Ti–V oxide ore

ABSTRACT

Secondary ion mass spectroscopy (SIMS) zircon and baddeleyite U–Pb ages, elemental, and Nd isotopic data are reported for the Zhuqing Fe–Ti–V oxide ore-bearing mafic intrusions in western Yangtze Block, South China. The mafic intrusions are dated at 1494 ± 6 Ma (zircon U–Pb), 1486 ± 3 Ma (baddeleyite U–Pb) and 1490 ± 4 Ma (baddeleyite U–Pb). The intrusions are dominantly gabbros that experienced variable degrees of alteration. All the studied rocks are high-Ti and alkaline in composition, and exhibit light rare earth element enrichment and "humped" incompatible trace-element patterns with no obvious Nb–Ta depletion, similar to intraplate alkali basaltic rocks in continental flood basalt (CFB) and ocean island basalt (OIB) provinces. Negative $\varepsilon_{Nd}(T)$ values (−0.97 to −3.58) and fractionation of the HREE of these rocks indicate that they were derived from a time-integrated, slightly enriched asthenospheric mantle source with minor crustal contamination. Like other Fe–Ti oxide mineralized rocks in plume-related layered intrusions or large igneous provinces around the world, the Zhuqing gabbros likely occurred in an intraplate setting. The ~1.5 Ga mafic magmatism was likely part of the global 1.6–1.2 Ga anorogenic magmatism related to the break-up of the supercontinent Nuna/Columbia, suggesting that the Yangtze Block may have been a component of the supercontinent.

© 2013 Elsevier B.V. All rights reserved.

1. Introduction

It has been widely accepted that Rodinia (ca. 900–700 Ma) and Pangea (ca. 320–170 Ma) were supercontinents resulting from the assembly of almost all of Earth's continents (Dalziel, 1995; Hoffman, 1991; Li and Evans, 2011; Li et al., 2008; Moores, 1991; Pesonen et al., 2003; Rogers, 1996). Most Rodinian fragments also contain abundant evidence to suggest that they contain parts of an even earlier supercontinent variously called Nuna (Evans and Mitchell, 2011; Hoffman, 1989, 1997; Zhang et al., 2012; we will use this name in the remainder of the paper for the late Paleo- to Mesoproterozoic supercontinent) or Columbia (Hou et al., 2008b; Meert, 2012; Rogers and Santosh, 2002; Zhao et al., 2002a). Efforts to reconstruct Nuna so far have been hampered by the small number of reliable paleomagnetic poles available (Buchan et al., 2001; Evans and Mitchell, 2011; Meert, 2002, 2012; Rogers, 2012; Rogers and Santosh, 2002, 2009; Zhang et al., 2012). Nonetheless, based on comparable global geological events, researchers consider that Nuna assembled along global 2.1–1.8 Ga collisional orogens, and its break-up was marked by widespread 1.6–1.2 Ga continental rifting, anorogenic magmatism and emplacement of mafic dyke swarms in almost all its cratonic building blocks (Condie, 2002; Ernst et al., 2008; Evans and Mitchell, 2011; Goldberg, 2010; Hou et al., 2008b; Rogers and Santosh, 2002; Zhang et al., 2012; Zhao et al., 2002a). Therefore, the identification of such global geological events may provide important constraints for piecing together the cratons that were once parts of the supercontinent.

The Yangtze Block played an important role in the reconstruction of the Rodinia supercontinent (e.g., Li et al., 1995, 2008), but little is known as to whether or not it was also a component of the Paleo- to Mesoproterozoic supercontinent Nuna. The Kongling Complex (marked as "1" in Fig. 1a) contains magmatic and metamorphic rocks as old as 3.3 Ga (Gao et al., 2011; Zhang et al., 2006a). Zheng et al. (2006) suggested a wide distribution of Archean rocks in the unexposed basement of the Yangtze Block based on U–Pb and Hf isotopic data from zircon xenocrysts in Paleozoic lamproites. Zhao et al. (2010) and Wang et al. (2012) reached the same conclusion based on detrital zircon

* Corresponding author. Tel.: +86 851 5895037; fax: +86 851 5891664.
E-mail address: zhuweiguang@vip.gyig.ac.cn (W.-G. Zhu).

0024-4937/$ – see front matter © 2013 Elsevier B.V. All rights reserved.
http://dx.doi.org/10.1016/j.lithos.2013.02.004

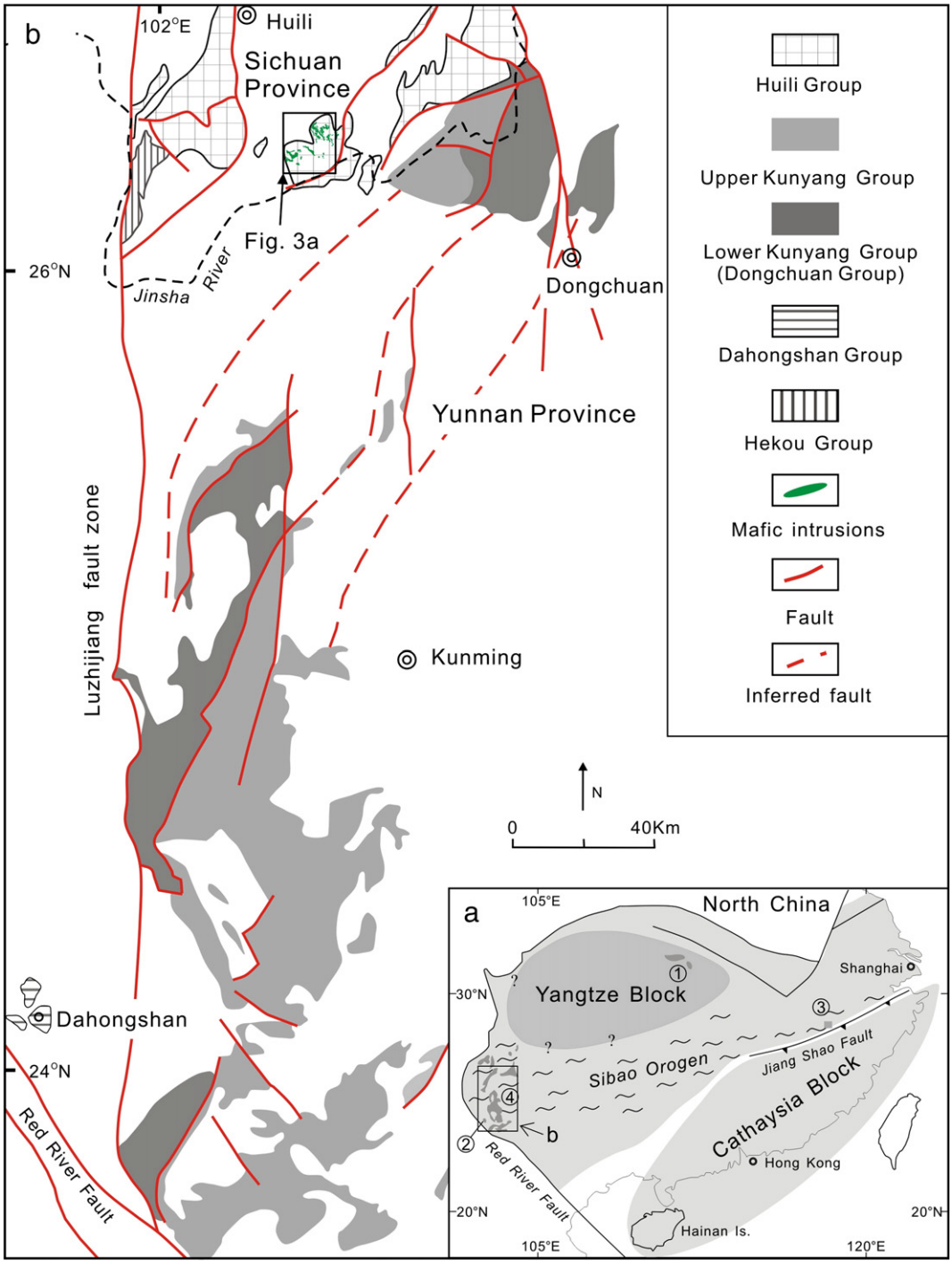

Fig. 1. a) Simplified tectonic map showing the study area in relation to South China's major tectonic units (Li et al., 2007). Numbers 1–4 indicate the Kongling Complex, the Dahongshan Group, the Tianli schists, and the Kunyang–Dongchuan Groups, respectively; b) geological map of the late Paleo- to Mesoproterozoic strata and Proterozoic intrusions in the Kangdian region, SW China.
Modified from Zhao and Zhou, 2011.

analyses of Paleo- to Neoproterozoic sedimentary rocks in southwestern Yangtze Block. In addition, 2.03–1.97 Ga granulites and 1.85 Ga A-type granites and mafic dykes have been identified in the northern part of the Yangtze Block (the Kongling Complex; "1" in Fig. 1a) (Peng et al., 2009, 2012; Sun et al., 2008; Wu et al., 2008; Xiong et al., 2009; Zhang et al., 2006b), which coincide with the age of Nuna assembly (Hoffman, 1989, 1997), and may therefore be genetically linked to the evolution of the supercontinent. Yao et al. (2011) presented evidence from detrital zircon U–Pb geochronology, Hf isotopes and geochemistry from South China (the Cathaysia Block, Fig. 1a) with clear age peaks at 1930–1520 Ma which they correlated with supercontinent Nuna. However, no Mesoproterozoic rocks in the Yangtze Block have previously been studied in detail and utilized for supercontinent reconstruction because of the paucity of known outcrops.

Apart from the Kongling Complex basement rocks that were stabilized at 1.85 Ga (Peng et al., 2012), there have been three other major Paleo- to Mesoproterozoic rock units previously reported from the Yangtze Block, including some volcanic and meta-volcanic rocks. The ca. 1.75–1.66 Ga Dahongshan Group (marked as "2" in Fig. 1a) consists of meta-volcaniclastic rocks, meta-basalts, meta-siliciclastic

rocks and marble (e.g., Greentree and Li, 2008; Zhao et al., 2010). The Tianli schists (marked as "3" in Fig. 1a) represent a clastic sedimentary succession, probably formed at the southern continental shelf of the Yangtze Block between ca. 1530 Ma and 1042 Ma (Li et al., 2007). The Kunyang–Dongchuan groups (marked as "4" in Fig. 1a) consist of a sequence of greenschist facies meta-sedimentary and meta-volcanic rocks that probably developed between 1.8–1.0 Ga (Greentree and Li, 2008; Greentree et al., 2006; Zhao et al., 2010).

No Mesoproterozoic mafic plutonic rocks have previously been reported for the Yangtze Block other than the report by geological mapping teams of a number of mafic intrusions that intrude dolomite and shales of the Mesoproterozoic Heishan Formation of the Huili Group in the Tong'an area, southwestern China (Fig. 1b). However, neither precise age nor geochemical characteristics of these rocks have yet been documented. In this study, we investigate the SIMS zircon and baddeleyite U–Pb ages, and elemental and Nd isotopic geochemistry of the Zhuqing Fe–Ti–V oxide ore-bearing mafic intrusions with the aim of (1) determining the precise crystallization age; (2) assessing the origin and nature of the parental magma, and the petrogenesis of these mafic intrusions; and (3) shedding new light on the regional magmatic–tectonic evolution during the late Paleo- to Mesoproterozoic, and possible genetic relationship between the Yangtze Block and the Nuna supercontinent.

2. Geological background and petrography

The South China Craton consists of two major Precambrian blocks: the Yangtze Block to the northwest and the Cathaysia Block to the southeast (present coordinates), with the late-Mesoproterozoic to earliest Neoproterozoic Sibao Orogen situated between them (Li et al., 2007) (Fig. 1a).

The Kangdian area (Fig. 1b) is located near the western margin of the Yangtze Block (Fig. 1a). The oldest supracrustal rocks in this area are the late Paleo- to Mesoproterozoic meta-volcanic and meta-sedimentary rocks, termed as the Dahongshan Group (Greentree and Li, 2008), the Dongchuan Group (Zhao et al., 2010), the Hekou Group (He, 2009; Zhao and Zhou, 2011), the Huili Group, and the Kunyang Group, which occur along the Luzhijiang fault and a series of related NNE-trending faults (Fig. 1b). They consist of meta-sedimentary rocks interbedded with felsic and mafic meta-volcanic rocks (Greentree and Li, 2008; Greentree et al., 2006; Li et al., 2002, 2006; Zhao et al., 2010). These late Paleo- to Mesoproterozoic rocks are overlain by a thick sequence (maximum >9 km) of Neoproterozoic (850–540 Ma) to Permian strata consisting of clastic, carbonate and volcanic rocks.

The ages of the Precambrian units in the Kangdian region had been poorly constrained until the availability of precise U–Pb zircon ages in recent years. Meta-volcanic units in the Dahongshan Group have been dated at 1675 ± 8 Ma and 1681 ± 13 Ma by SHRIMP zircon U–Pb (Greentree and Li, 2008) and LA-ICP-MS zircon U–Pb (Zhao and Zhou, 2011) methods, respectively, which are slightly older than a 1659 ± 16 Ma LA-ICP-MS zircon U–Pb age for a dolerite dyke intruding the sequence (Zhao and Zhou, 2011). The Hekou Group in the northwestern part of the study region (Fig. 1b) is a sequence of meta-clastic and meta-carbonate rocks, and is generally considered to be the equivalent of the Dahongshan Group (e.g., Zhao et al., 2010), as confirmed by a recent SHRIMP zircon U–Pb age of 1695 ± 20 Ma for meta-volcanic rocks from the Hekou Group (He, 2009) (Figs. 1 and 2).

The Kunyang Group in the southern part of the study region (Fig. 1b) was divided into the Upper and Lower Kunyang groups (e.g., Zhao and Zhou, 2011; Zhao et al., 2010). From the base upward, the Lower Kunyang Group, also called as the Dongchuan Group (Zhao and Zhou, 2011; Zhao et al., 2010), includes the Yinmin, Luoxue, E'touchang, and Luzhijiang formations, whereas the Upper Kunyang Group consists of the Dayingpan, Heishantou, Dalongkou, and Meidang formations (Fig. 2). Detrital zircons from the Dongchuan Group yielded the youngest age of ~1.78 Ga and a tuff sample from the same group has a zircon U–Pb age of 1742 ± 13 Ma (Zhao et al., 2010). Sun et al. (2009b) reported a SHRIMP zircon age of 1503 ± 17 Ma for a tuff sample from the E'touchang Formation in the Lower Kunyang Group. Thus, the Lower Kunyang Group likely formed between ~1.7 and ~1.5 Ga. Zhao et al. (2010) hence interpreted the Dongchuan and Dahongshan groups as stratigraphically correlatable units (Fig. 2).

Tuff layers in the Heishantou Formation of the Upper Kunyang Group have been dated at 995 ± 15 Ma and 1032 ± 9 Ma by the SHRIMP zircon U–Pb method (Greentree et al., 2006; Zhang et al., 2007). Detrital zircons from the top of the Kunyang Group also gave U–Pb ages as young as 960 Ma (Greentree et al., 2006; Sun et al., 2009a).

The Huili Group in the northern part of the study region (Fig. 1b) is a >10 km-thick sequence of meta-clastic and meta-carbonate rocks interbedded with volcanic rocks. The group consists of the Yinmin, Luoxue, Heishan, Qinglongshan, Limahe, Fengshan, and Tianbaoshan Formations, from the base upward. The meta-volcanic rocks in the Tianbaoshan Formation yield TIMS zircon U–Pb and SHRIMP zircon U–Pb ages of 1028 ± 9 Ma (Geng et al., 2007).

More than 25 mafic intrusions, including the Zhuqing intrusions, crop out in the Tong'an area, Huili County, southwestern China (Figs. 1b and 3a). These intrusions, dominantly composed of gabbroic rocks, occur as dykes or small irregular intrusions that intrude the dolomite or shales of the Mesoproterozoic Heishan Formation, the Huili Group (Fig. 3). The mafic intrusions are up to four kilometers long and commonly 90–370 m wide, striking NW 300°–350°. Intrusions I and II host Fe–Ti–V oxide ore-bearing deposits, whereas intrusion III, the largest one in this area, has no reported mineralization (Fig. 3b). Most of the intrusions consist of medium- to coarse-grained gabbros (Fig. 4). These gabbros are mainly composed of anhedral crystals of plagioclase, clinopyroxene, Fe–Ti oxides (magnetite and ilmenite), and minor amounts of hornblende, biotite, apatite, and sulfide minerals (pyrite and chalcopyrite). Most of the intrusions experienced variable degrees of alteration, resulting in albitization of some plagioclases and some clinopyroxenes altered to amphibole or chlorite (Fig. 4b). The ore-barren gabbros consist of 40–60 vol.% plagioclase, 30–40 vol.% clinopyroxene, 5–10 vol.% Fe–Ti oxides and minor amounts of hornblende, biotite, sulfide minerals and apatite (Fig. 4b). The Fe–Ti–V oxide ore-bearing gabbros consist of approximately 20 vol.% Fe–Ti oxides (magnetite and ilmenite), 40 vol.% plagioclase, 30 vol.% clinopyroxene, and minor amounts of hornblende and sulfide minerals (pyrite and chalcopyrite) (Fig. 4c and d).

3. Sampling and analytical methods

Thirty samples were collected from four drill cores (ZK2801, ZK3601, ZK704, and ZK001; Fig. 3b) and surface outcrops (samples with JQ names in Fig. 3b) for the three representative intrusions (I, II, and III) in the Tong'an area (Fig. 3b). Zircons from samples JQ1010, and baddeleyites from samples JQ1002 and JQ1010, were separated using conventional heavy liquid and magnetic techniques, then by handpicking under binocular microscopes. They were mounted in an epoxy resin disk, and polished and coated with gold film. Both zircons and baddeleyites were documented with transmitted and reflected light micrographs as well as cathodoluminescence (CL) and backscattered electron images to reveal their external and internal structures. Zircon and baddeleyite U–Pb dating were conducted using a Cameca IMS 1280 ion microprobe (SIMS) at the Institute of Geology and Geophysics, the Chinese Academy of Sciences (CAS) in Beijing. Details of the analytical procedures for zircon and baddeleyite U–Pb dating can be found in Li et al. (2009) and Li et al. (2010), respectively. Oxygen flood that introduces oxygen into the sample chamber was used during the analyses, which not only enhances Pb^+ ion yield by a factor of 2 and 7 for zircon and baddeleyite (Li et al., 2009, 2010), respectively, but also depresses the U–Pb orientation effect (Wingate

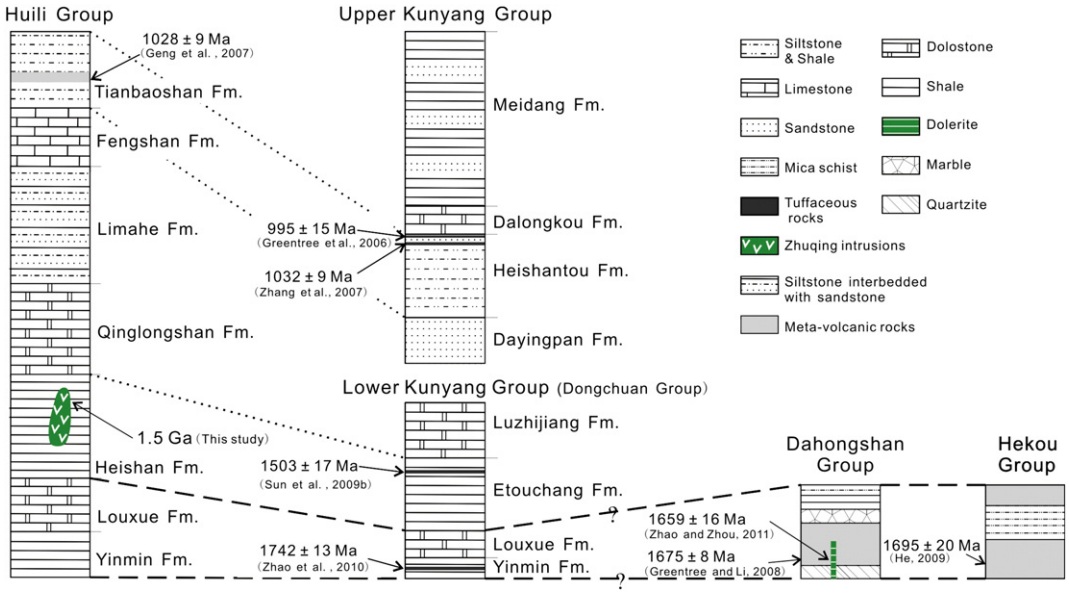

Fig. 2. Simplified stratigraphic correlation for the Proterozoic strata in the western Yangtze Block, SW China. Modified after Greentree et al., 2006 and Zhao and Zhou, 2011.

and Compston, 2000) down to ~2% (Li et al., 2010). All baddeleyites were mounted in random orientations due to their small sizes and polysynthetic twinning. The uncertainties in ages are cited as 1σ, and the weighted mean ages are quoted at the 95% confidence interval (2σ). The SIMS U–Pb zircon and baddeleyite ages are presented in Appendix A.

Major element compositions of whole rocks were determined using X-ray fluorescence spectrometers (XRF) at either the State Key Laboratory of Isotope Geochemistry, Guangzhou Institute of Geochemistry of CAS, or ALS Chemex Co Ltd, Guangzhou. The analytical precision was better than 5%. Trace elements in whole rocks were analyzed using a Perkin-Elmer Sciex ELAN DRC-e ICP-MS at the State Key Laboratory of Ore Deposit Geochemistry (SKLOG), Institute of Geochemistry of CAS. The powdered samples (50 mg) were dissolved with $HF+HNO_3$ mixture in high-pressure Teflon bombs at ~190 °C for 48 h (Qi et al., 2000). Rh was used as an internal standard to monitor signal drift during measurement. The international standards GBPG-1, OU-6, and the Chinese National standards GSR-1 and GSR-3, were used for analytical

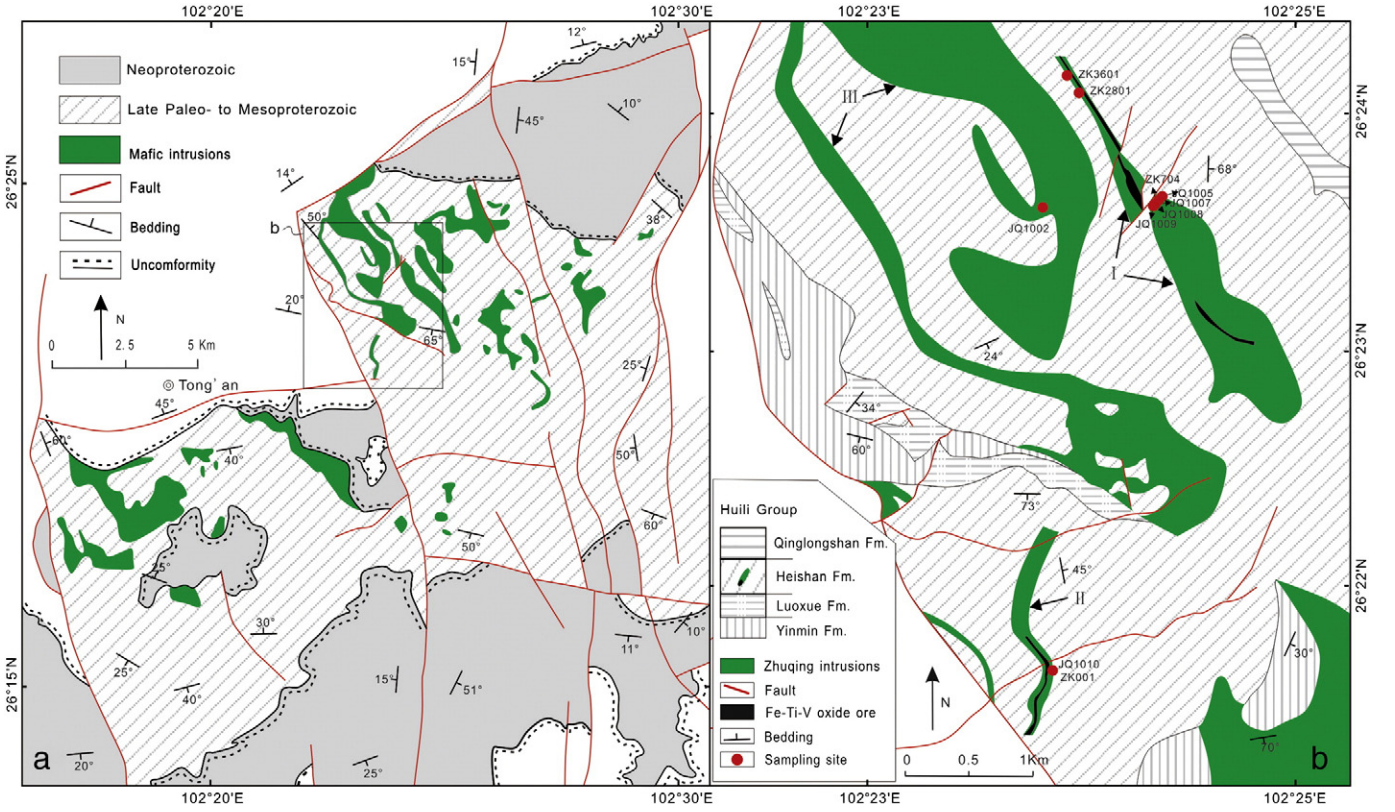

Fig. 3. a) Simplified geological map of the Mesoproterozoic to earliest Neoproterozoic rocks in the Tong'an region; b) geological map of the Zhuqing intrusions and sampling location.

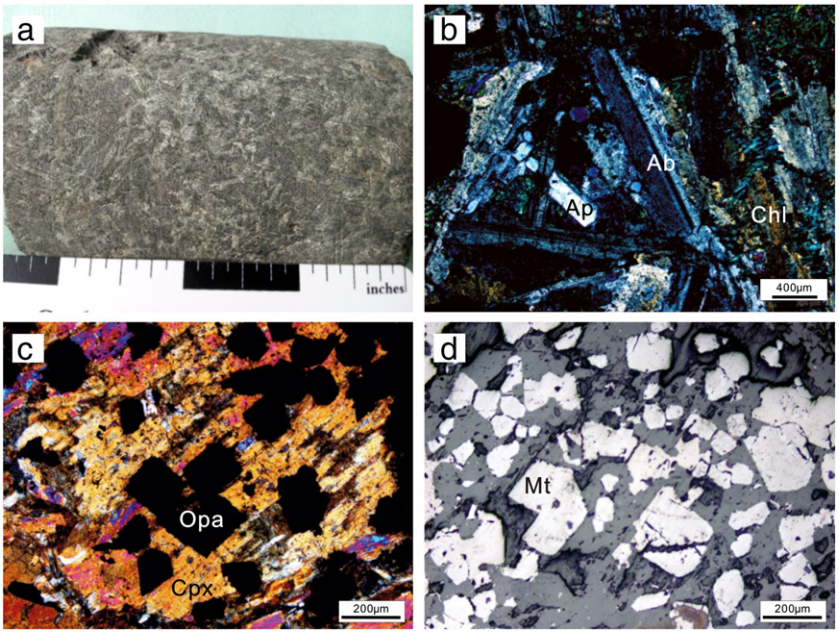

Fig. 4. Hand specimen and microscopic photographs of gabbros from the Zhuqing intrusions. a) Sample from drill core showing the gabbroic structure; b) microphotographs of minerals with hydrothermal alteration; c) and d) microphotographs of Fe–Ti–V oxide ore-bearing gabbros. Ap = Apatite; Ab = Albite; Chl = Chlorite; Opa = Magnetite/Ilmenite; Mt = Magnetite.

quality control. The analytical precision was generally better than 10% for trace elements. Major and trace element compositions for the thirty samples are presented in Table 1.

Samples for Nd isotopic analysis were spiked and dissolved with $HF + HNO_3$ acid in Teflon bombs. Sm and Nd were separated by conventional cation-exchange techniques. The isotopic measurements were performed on a Thermal Ionization Mass Spectrometry (TIMS) — Triton at the SKLODG. The measured $^{143}Nd/^{144}Nd$ ratios were normalized to $^{146}Nd/^{144}Nd = 0.7219$. The $^{143}Nd/^{144}Nd$ ratios of the USGS standard rock BCR-2 determined during this study were 0.512622 ± 0.000004 (2σ).

4. Results

4.1. U–Pb zircon and baddeleyite geochronology

4.1.1. Zircon age for sample JQ1010

Zircons are clear and up to 50–150 μm in length with length to width ratios between 1:1 and 2:1. Most zircons are simple prismatic crystals without obvious zoning under CL (Fig. 5a). Seventeen analyses were conducted on 17 zircons (Appendix A). Uranium and thorium concentrations are variable, with U = 87–2847 ppm, Th = 26–5967 ppm and Th/U = 0.30–1.45 with the exception of a very high Th/U value of 5.75 for spot 9. Most analyses yielded near concordant ages, while three grains are obviously discordant due to progressive loss of radiogenic lead from the original magmatic zircons. All 17 analyses yield a discordia line with an upper intercept age of 1499 ± 7 Ma and a lower intercept age of 299 ± 15 Ma (MSWD = 0.79) which probably reflects a late-stage thermal disturbance. Fourteen of the seventeen analyses give consistent $^{207}Pb/^{206}Pb$ ratio within errors, yielding a weighted average $^{207}Pb/^{206}Pb$ age of 1494 ± 6 Ma (2σ, MSWD = 0.59) (Fig. 6).

4.1.2. Baddeleyite ages for samples JQ1002 and JQ1010

Baddeleyites from sample JQ1002 are mostly anhedral, ranging from 30 to 150 μm in length, and have length to width ratios between 1:1 and 2:1 (Fig. 5b). Eighteen analyses were conducted on 18 grains during a single analytical session. Measured uranium concentrations are high, varying from 827 to 4542 ppm, and thorium contents range from 20 to 538 ppm, with Th/U ratios of 0.02–0.12 (Appendix A). All 18 measurements are concordant in U–Pb isotopic systems, yielding a weighted average $^{207}Pb/^{206}Pb$ age of 1486 ± 3 Ma (2σ, MSWD = 1.2) (Fig. 7a). This age is considered as the best estimate of the crystallization age for sample JQ1002.

Baddeleyites from sample JQ1010 are also mostly anhedral, ranging from 50 to 200 μm in length with length to width ratios ranging between 1:1 and 2:1 (Fig. 5c). Twenty-five analyses give variable concentrations of U (62 to 2319 ppm) and Th (1 to 132 ppm), with Th/U ratios of 0.01–0.08 (Appendix A). All the 25 analyses give near-concordant U–Pb results (Fig. 7b). The weighted mean $^{207}Pb/^{206}Pb$ age is 1490 ± 4 Ma (95% confidence interval, MSWD = 0.47), which is interpreted as the best estimate of the crystallization age for sample JQ1010. This age is consistent with its zircon U–Pb age of 1494 ± 6 Ma (Fig. 6) within analytical uncertainties, suggesting that metamorphism and alteration did not significantly affect the zircon and baddeleyite U–Pb isotope systems. Thus, the age of ~1.5 Ga represents the crystallization age for sample JQ1010.

4.2. Geochemical and Nd isotopic characteristics

4.2.1. Alteration effects on chemical compositions

Major and trace element data for the Zhuqing mafic intrusions are listed in Table 1. All the samples in this study have undergone variable degrees of alteration, which is consistent with the variable LOI (loss of ignition) values (0.91–3.08 wt.%). Thus, the effects of alteration on chemical compositions of these rocks need to be evaluated. Zirconium in mafic igneous rocks is generally considered to be most immobile during low- to medium-grade alteration (e.g., Wood et al., 1979). Therefore, bivariate plots of Zr against selected trace elements have been used for evaluating the motilities of such elements during alteration (e.g., Polat et al., 2002). A number of elements with different geochemical behaviors, including Nb, Y, Th, V, Rb, Sr, Ba and Pb in the Fe–Ti–V oxide ore-barren rocks, are plotted against Zr to evaluate their mobility during alteration (Fig. 8). High-field strength elements (HFSE: Y, Nb, and Th) except Pb, rare earth elements (REEs), and siderophile elements (such as V) correlated tightly with Zr, indicating that these elements are essentially immobile during alteration. In contrast, large-ion lithophile elements (LILE: Rb, Sr, and Ba) and Pb

Table 1
Major element (in wt.%) and trace element (in ppm) data of the Zhuqing intrusions.

Sample no.	JQ1002	JQ1005	JQ1007	JQ1008	JQ1009	JQ1010	ZK2802	ZK2804	ZK2807	ZK2813	ZK2817	ZK2821	ZK2824	ZK2828	ZK2841
Rock name	Gab	Gab	Gab	Gab	Gab	Gab	Ore	Ore	Ore	Gab	Ore	Ore	Ore	Gab	Gab
Body	III	I	I	I	I	II	I	I	I	I	I	I	I	I	I
SiO_2	44.77	47.96	45.90	46.30	41.77	42.88	29.17	24.84	37.15	40.50	27.85	31.46	33.47	37.60	43.32
TiO_2	4.26	2.95	4.53	4.85	4.70	3.42	7.77	10.49	5.82	5.10	8.86	7.31	6.85	5.54	4.69
Al_2O_3	12.24	15.11	12.15	12.72	12.40	13.44	7.14	5.31	11.09	12.10	6.32	9.28	10.79	12.00	12.27
Fe_2O_3	20.49	14.32	19.11	16.51	23.20	20.36	36.97	42.55	28.12	23.37	39.51	33.02	30.61	25.00	20.04
MnO	0.26	0.14	0.23	0.28	0.22	0.26	0.38	0.45	0.34	0.33	0.51	0.38	0.32	0.29	0.20
MgO	4.11	3.65	4.15	4.35	4.90	5.97	8.45	9.09	5.86	5.36	9.46	7.95	7.20	6.50	4.33
CaO	7.12	9.12	6.71	8.88	5.56	7.38	4.72	4.37	4.96	6.20	4.65	5.19	4.64	5.81	7.11
Na_2O	2.92	3.92	3.33	3.37	2.47	2.51	0.29	0.23	2.22	2.99	0.14	0.81	1.63	2.27	3.28
K_2O	1.57	0.40	1.25	0.31	1.97	1.01	1.02	0.12	1.58	1.16	0.20	1.58	1.56	1.41	1.21
P_2O_5	0.44	0.42	0.43	0.37	0.35	0.27	0.20	0.16	0.30	0.41	0.21	0.21	0.25	0.32	0.50
LOI	1.49	1.70	1.89	1.75	2.14	2.18	3.08	1.36	2.10	2.26	2.32	2.23	2.61	2.90	3.02
Total	99.67	99.69	99.69	99.69	99.69	99.69	99.19	98.97	99.54	99.78	100.03	99.42	99.93	99.64	99.97
Mg#	28.4	33.6	30.1	34.3	29.5	36.8	31.2	29.7	29.2	31.2	32.2	32.3	31.8	34.0	30.0
Sc	40.3	40.8	44.8	48.0	33.8	25.2	25.2	22.1	25.5	29.9	23.5	23.5	25.6	27.5	33.4
V	194	373	209	334	385	408	1410	2410	707	454	1560	1240	1120	789	298
Cr	7	25	6	6	59	40	405	895	90	32	574	464	347	117	8
Co	43	32	38	38	50	65	105	111	71	58.8	125	111	101	85	40
Ni	22	26	20	9	62	96	234	319	107	67	260	210	174	120	36
Cu	88	39	112	46	106	105	56	58	73	94	64	52	77	113	48
Zn	217	119	218	459	260	181	288	258	282	309	291	297	359	242	314
Ga	25.4	20.6	22.8	18.9	23.6	24.0	21.3	24.0	21.3	23.0	21.3	22.7	22.8	23.7	23.0
Rb	65.9	6.18	51.5	4.69	85.4	25.5	37.5	3.27	56.1	45.0	5.91	51.6	49.3	51.9	49.2
Sr	178	575	126	123	53.7	278	23.3	23.6	88.2	133	19.1	42.1	68.1	123	124
Y	43.3	36.4	44.3	41.8	31.8	30.0	19.7	17.9	28.5	36.5	16.1	18.7	23.2	29.0	47.3
Zr	274	170	254	250	199	185	128	106	178	229	114	133	142	176	280
Nb	45.9	35.1	45.2	50.8	34.1	32.5	22.4	20.3	30.4	37.3	20.8	22.5	23.7	30.8	46.2
Cs	6.18	0.45	4.61	0.43	7.33	1.67	3.97	0.23	8.05	6.01	0.68	5.14	7.09	6.42	5.98
Ba	708	153	498	140	767	321	326	34	428	286	44	465	389	337	442
La	37.60	30.30	35.20	31.70	28.70	30.50	20.30	12.20	27.30	36.70	20.30	20.90	21.50	22.60	49.70
Ce	84.50	59.20	78.30	70.20	64.80	61.60	40.10	23.00	55.70	75.10	39.10	41.20	43.00	47.00	99.80
Pr	9.60	7.74	8.83	8.09	7.32	7.59	5.00	3.18	6.98	9.29	4.77	5.00	5.30	5.89	12.10
Nd	39.70	31.50	36.80	32.70	29.60	30.70	20.10	13.00	29.10	38.30	19.10	20.00	22.00	24.00	49.70
Sm	8.51	6.79	8.37	7.48	6.45	6.25	4.19	2.75	6.49	8.26	3.74	4.21	4.99	5.44	11.00
Eu	2.87	2.41	2.83	2.53	2.51	2.02	1.33	0.57	1.53	2.27	0.69	1.45	1.48	1.60	3.55
Gd	9.62	6.77	9.05	7.93	6.99	6.60	4.10	2.82	6.38	7.72	3.47	4.26	4.67	5.44	10.40
Tb	1.46	1.08	1.48	1.31	1.15	0.98	0.71	0.47	1.10	1.31	0.61	0.71	0.82	0.95	1.80
Dy	8.20	6.27	8.30	7.56	6.07	5.34	3.94	2.72	5.99	7.23	3.37	3.82	4.60	5.20	10.00
Ho	1.80	1.37	1.78	1.70	1.29	1.17	0.85	0.60	1.33	1.58	0.71	0.80	0.99	1.13	2.10
Er	4.63	3.51	4.75	4.48	3.54	3.09	2.35	1.56	3.59	4.36	2.00	2.21	2.66	3.00	5.72
Tm	0.66	0.50	0.66	0.65	0.48	0.43	0.34	0.22	0.49	0.58	0.27	0.30	0.36	0.42	0.77
Yb	4.27	3.17	4.30	4.21	3.22	2.81	2.17	1.49	3.15	3.88	1.79	2.06	2.40	2.65	5.06
Lu	0.64	0.47	0.64	0.61	0.47	0.42	0.31	0.20	0.46	0.56	0.27	0.28	0.35	0.39	0.74
Hf	6.66	4.14	6.59	5.88	4.93	4.40	3.72	2.43	5.14	6.32	3.23	3.60	3.95	4.24	7.82
Ta	3.00	1.89	2.85	3.57	2.26	1.78	1.61	1.29	2.25	2.69	1.57	1.72	1.68	1.70	3.31
Pb	2.27	4.12	1.38	2.67	1.94	3.52	2.84	5.55	1.96	3.10	3.83	1.86	2.16	1.63	2.49
Th	4.37	2.66	4.50	4.70	3.54	2.99	1.74	1.86	2.99	3.76	1.66	2.12	2.25	2.46	5.03
U	0.88	0.57	0.89	1.04	0.77	0.63	0.44	0.34	0.66	0.78	0.37	0.43	0.48	0.48	1.06

$Mg^{\#} = 100 * \text{molar MgO}/(Mg + FeO_T)$, assuming $FeO_T = 0.9 * Fe_2O_3$, Total iron as FeO_T. LOI = loss on ignition, Gab = Fe–Ti–V oxide ore-barren gabbro; Ore = Fe–Ti–V ore-bearing gabbro.

are overall scattered, implying varying degrees of mobility caused by the alteration. Although the correlation of major oxides with MgO contents (Fig. 9) suggests that the effects of alteration on major oxides are minor (Fig. 8), the sums of major element oxides for all samples are still recalculated to 100% volatile free. Only immobile elements are used for geochemical classification and petrogenetic discussions.

4.2.2. Geochemical characteristics

The Fe–Ti–V oxide ore-barren gabbros of the Zhuqing intrusions display variable Fe_2O_3, TiO_2, MgO, V Cr, and Ni contents, with variably low SiO_2 contents (Table 1). In contrast, the Fe–Ti–V oxide ore-bearing gabbros from the Zhuqing intrusions have higher Fe_2O_3, TiO_2, MgO, V, Cr and Ni, and lower SiO_2 concentrations than those of the ore-barren gabbros (Table 1). All the samples show evolved compositions with variable $Mg^{\#}$ number of 24.0–37.8. Fe_2O_3, TiO_2, Cr and Ni contents increase, whereas SiO_2, Al_2O_3, CaO and total alkalis ($Na_2O + K_2O$) contents decrease, with increasing MgO contents (Fig. 9). On the TAS rock classification diagram, these ore-barren rocks from the Zhuqing intrusions plot in the alkaline field (Fig. 10). The ore-barren rocks are characterized by high ratios of Ti/Y (305–1311, mostly >500). Fe–Ti–V oxide ore deposits are typically generated from high-Ti parental magma; for example, all the Fe–Ti–V oxide ore deposits in the Emeishan large igneous province (ELIP) have been suggested to have crystallized from basaltic magmas rich in TiO_2 (e.g., Zhou et al., 2008). Therefore, the Zhuqing gabbroic intrusions were also likely related to high-Ti alkaline basaltic magma (e.g., Xu et al., 2001).

Despite variable REE abundances, the samples from the Zhuqing mafic intrusions display parallel REE patterns with enrichments in light rare earth elements (LREEs) and depletions in heavy rare earth elements (HREEs) [$(La/Yb)_N = 5.1–7.8$; Subscript N denotes the chondrite-normalized] (Boynton, 1984) (Fig. 11a). Among them, the

ZK2851	ZK3601	ZK3619	ZK0401	ZK0402	ZK0403	ZK0404	ZK0406	ZK0407	ZK0408	ZK0101	ZK0102	ZK0103	ZK0104	ZK0105
Gab	Gab	Gab	Ore	Ore	Ore	Ore	Gab	Gab	Gab	Gab	Gab	Gab	Gab	Gab
I	I	I	I	I	I	I	I	I	I	II	II	II	II	II
45.99	40.06	43.07	34.29	35.69	30.55	28.78	44.92	47.40	48.59	38.79	39.99	39.67	40.00	42.15
4.44	4.65	3.52	6.46	5.94	7.61	9.03	3.86	3.68	3.10	4.30	4.52	4.26	4.39	3.97
11.31	12.54	14.00	9.08	10.60	8.89	5.53	13.80	11.73	12.09	12.44	12.43	12.45	12.47	13.29
19.70	21.95	18.94	30.27	29.26	35.10	38.62	18.34	17.80	18.97	23.46	23.38	23.69	23.35	20.71
0.26	0.24	0.29	0.31	0.30	0.29	0.30	0.20	0.20	0.21	0.26	0.26	0.24	0.24	0.34
3.14	5.29	4.85	7.20	6.47	7.16	9.98	4.17	4.29	3.21	7.12	6.90	6.93	6.88	6.35
8.38	6.76	7.26	6.89	5.88	5.32	5.23	7.43	8.62	6.41	7.60	6.73	6.81	6.80	6.89
3.51	2.27	3.20	0.65	1.57	0.76	0.18	3.37	3.38	3.94	1.48	2.23	2.13	2.24	2.31
1.57	2.21	1.26	1.70	1.08	1.50	0.24	0.93	0.80	1.59	1.56	0.65	0.84	0.70	1.38
0.61	0.40	0.379	0.28	0.29	0.23	0.16	0.42	0.44	0.67	0.23	0.26	0.25	0.25	0.28
1.00	2.18	2.12	2.52	2.59	2.22	1.57	2.26	1.34	0.91	2.43	2.35	2.43	2.38	2.01
99.92	98.56	98.88	99.66	99.67	99.62	99.61	99.70	99.68	99.68	99.68	99.69	99.69	99.70	99.68
24.0	32.3	33.7	32.0	30.5	28.8	33.9	31.1	32.3	25.1	37.5	36.9	36.7	36.9	37.8
42.1	32.0	15.5	26.3	26.1	22.9	20.8	62.2	61.8	33.4	19.1	23.2	20.7	21.6	17.9
139	618	345	819	775	1080	1430	187	285	48.2	562	564	556	563	426
3	78	17	95	91	366	496	7	15	8	69	61	63	62	19
35	58	47	97	82	105	131	34	33	33	87	83	81	83	64
11	71	34	145	132	179	219	14	12	5	135	134	130	132	106
183	46	81	76	77	64	66	101	105	152	55	90	70	74	73
231	209	633	286	301	241	261	157	262	258	178	217	198	198	202
25.2	26.5	23.6	22.7	23.5	21.3	18.1	22.6	18.5	25.4	21.4	21.5	22.0	22.3	22.1
45.0	85.6	44.0	78.9	48.2	57.8	7.17	20.0	20.3	57.2	43.2	16.7	22.9	18.1	43.6
148	149	324	75.4	123	42.4	22.6	222	228	155	301	376	357	374	298
53.7	37.8	32.7	26.8	26.7	21.3	18.4	44.5	45.9	61.7	20.2	23.4	22.9	22.9	25.6
289	216	220	164	159	134	119	255	248	394	124	147	141	143	167
47.2	40.0	38.6	30.1	28.5	24.1	25.3	39.2	40.7	60.2	21.9	25.0	24.6	24.9	29.6
4.33	10.2	3.27	9.82	5.83	7.96	0.69	1.63	0.70	4.92	3.62	1.10	1.67	1.13	3.18
625	406	464	444	288	406	49.4	249	252	535	454	227	273	226	481
48.30	35.90	35.20	25.40	24.60	17.30	21.80	39.10	40.70	57.50	19.70	22.30	22.50	22.30	26.60
99.80	72.80	71.00	56.10	54.70	40.00	46.00	88.00	82.30	106.00	44.20	49.40	50.50	49.70	59.20
12.60	9.07	8.81	6.24	6.15	4.44	4.89	10.10	10.60	15.00	4.91	5.50	5.48	5.43	6.50
51.60	37.80	34.50	25.00	24.70	19.00	19.50	40.70	43.20	59.60	19.40	22.10	21.70	21.90	25.80
11.00	7.95	7.19	5.30	5.44	4.25	3.83	8.99	9.66	12.70	4.02	4.69	4.75	4.65	5.45
3.22	2.67	2.20	1.78	1.75	1.58	1.06	3.08	2.87	3.67	1.64	1.73	1.78	1.72	2.05
11.10	8.34	7.19	5.82	5.79	4.92	4.05	9.57	10.19	13.40	4.44	5.03	5.00	4.95	5.61
1.86	1.34	1.13	0.90	0.89	0.71	0.64	1.54	1.59	2.17	0.70	0.79	0.78	0.79	0.90
10.80	7.32	6.25	5.09	5.03	3.95	3.51	8.55	8.78	12.00	3.75	4.43	4.34	4.29	4.89
2.30	1.42	1.23	1.09	1.09	0.86	0.76	1.85	1.76	2.55	0.81	0.91	0.92	0.94	1.04
6.32	4.14	3.58	2.99	3.01	2.33	2.02	4.90	5.02	6.92	2.18	2.49	2.47	2.51	2.79
0.86	0.56	0.49	0.41	0.40	0.33	0.30	0.68	0.69	0.98	0.30	0.34	0.34	0.36	0.37
5.60	3.67	3.21	2.72	2.67	2.04	1.88	4.35	4.33	6.08	1.94	2.19	2.19	2.29	2.46
0.84	0.57	0.47	0.39	0.40	0.30	0.28	0.62	0.64	0.89	0.30	0.32	0.32	0.34	0.37
7.98	5.33	5.17	4.35	4.20	3.36	3.05	6.70	6.60	9.52	3.12	3.57	3.56	3.63	4.12
3.13	2.67	2.52	2.17	1.93	1.65	1.69	2.51	2.98	3.85	1.44	1.59	1.59	1.62	1.94
1.68	1.66	4.76	2.83	2.13	1.89	3.48	3.02	2.37	10.61	1.76	2.51	2.49	2.51	6.83
4.69	3.76	3.73	3.10	2.81	2.17	1.61	4.29	4.46	6.63	2.26	2.39	2.60	2.57	3.15
1.03	0.76	0.73	0.66	0.61	0.49	0.43	0.88	0.92	1.33	0.46	0.51	0.53	0.53	0.63

Fe–Ti–V oxide ore-bearing gabbros have lower total REE contents. In the primitive mantle-normalized multi-element plot (Fig. 11b), all the samples from the Zhuqing mafic intrusions have "humped" patterns characterized by variable enrichment in all incompatible elements. Moreover, no sample exhibits obvious Nb–Ta depletion (Nb/La = 0.93–1.66), resembling typical intraplate alkali basaltic rocks in CFB and OIB provinces (Sun and McDonough, 1989). The Fe–Ti–V oxide ore-bearing samples exhibit large positive Ti anomalies due to variable degrees of accumulation of Fe–Ti oxides (Fig. 11b).

4.2.3. Nd isotopes

Samples from the Zhuqing intrusions display limited variations in the Sm–Nd isotopic compositions (Table 2). Their $(^{143}Nd/^{144}Nd)_i$ ratios range from 0.510529 to 0.510663, corresponding to $\varepsilon_{Nd}(T)$ values ranging from −0.97 to −3.58. These Nd isotopic compositions suggest that the parental magmas of the Zhuqing gabbros were derived from a time-integrated slightly enriched mantle source.

5. Discussions

5.1. Crystallization age of the Zhuqing intrusions

Baddeleyite has long been considered an ideal geochronometer for dating crystallization ages of mafic-ultramafic rocks by the U–Pb isotopic method (see Rodionov et al., 2012 and references therein). Thus, the two baddeleyite ages of 1486 ± 3 Ma and 1490 ± 4 Ma from the Zhuqing intrusions are probably the best estimate of the crystallization ages for these rocks.

Zircon formed in magmatic and metamorphic processes might be altered by later aqueous fluids or hydrous melts, resulting in partial or

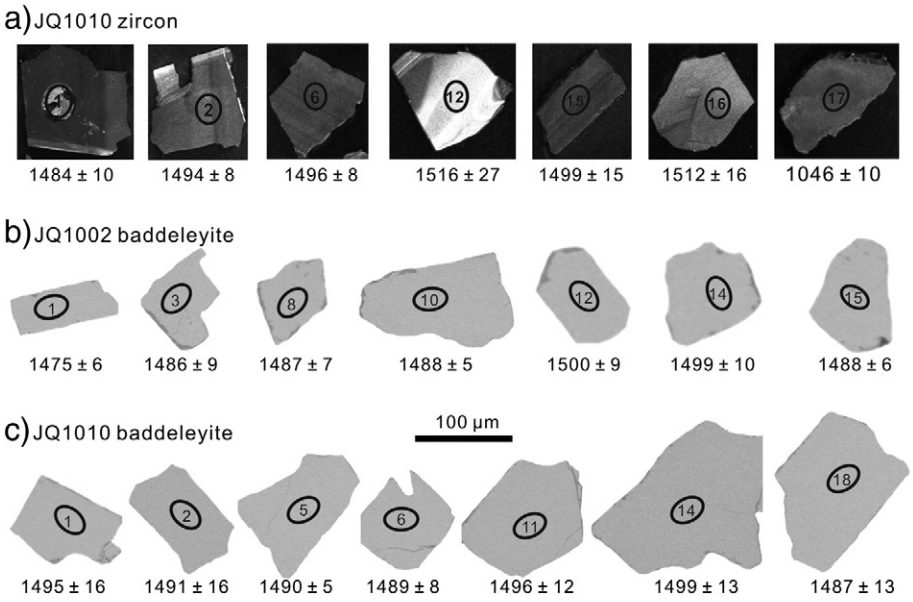

Fig. 5. Transmitted CL images of representative zircons from sample JQ1010 (N 26°21′30.6″, E 102°23′49.3″) (a), and backscattered electron images of baddeleyites from sample JQ1002 (N 26°23′35.7″, E 102°23′50.5″) (b) and JQ1010 (c). $^{207}Pb/^{206}Pb$ ages for the spots on representative grains are shown in Ma with 1σ errors.

total loss of radiogenetic Pb (e.g., Chen et al., 2010 and references therein). However, it is generally accepted that magmatic and metamorphic zircons can be distinguished by their Th/U ratios (Hoskin and Schaltegger, 2003). Zircons from the Zhuqing intrusions have relatively high Th/U ratios (Appendix A), together with their CL images (Figs. 5a), suggesting a magmatic origin. The mean weighted average $^{207}Pb/^{206}Pb$ age (1494 ± 6 Ma) of zircons is consistent with the baddeleyites U–Pb ages within errors. This age of ~1.5 Ga age, taken as the best estimate of the crystallization age for the Zhuqing intrusions, is also consistent with the 1503 ± 17 Ma age of a tuff sample from the E'touchang Formation of the Lower Kunyang Group (Sun et al., 2009b) (Fig. 2).

5.2. Petrogenesis of the Zhuqing mafic intrusions

5.2.1. Fractional crystallization and crustal contamination

The Zhuqing gabbroic intrusions exhibit variable MgO concentrations, suggesting that they have undergone fractional crystallization to various degrees, as shown by similar evolutionary trends on some element diagrams (Fig. 9).

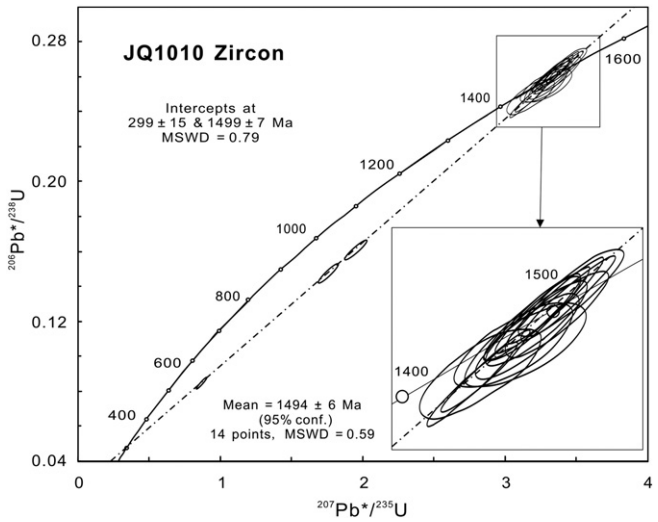

Fig. 6. Zircon U–Pb Concordia diagrams of sample JQ1010 from the Zhuqing intrusions.

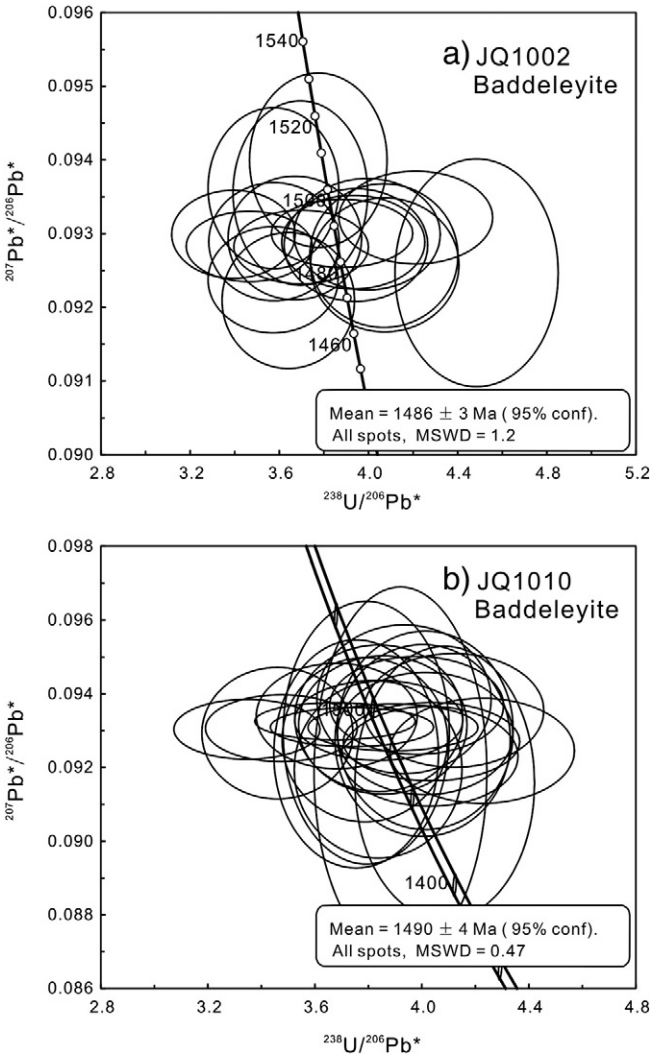

Fig. 7. Baddeleyite U–Pb Concordia diagrams of sample (a) JQ1002 and (b) JQ1010 from the Zhuqing gabbros.

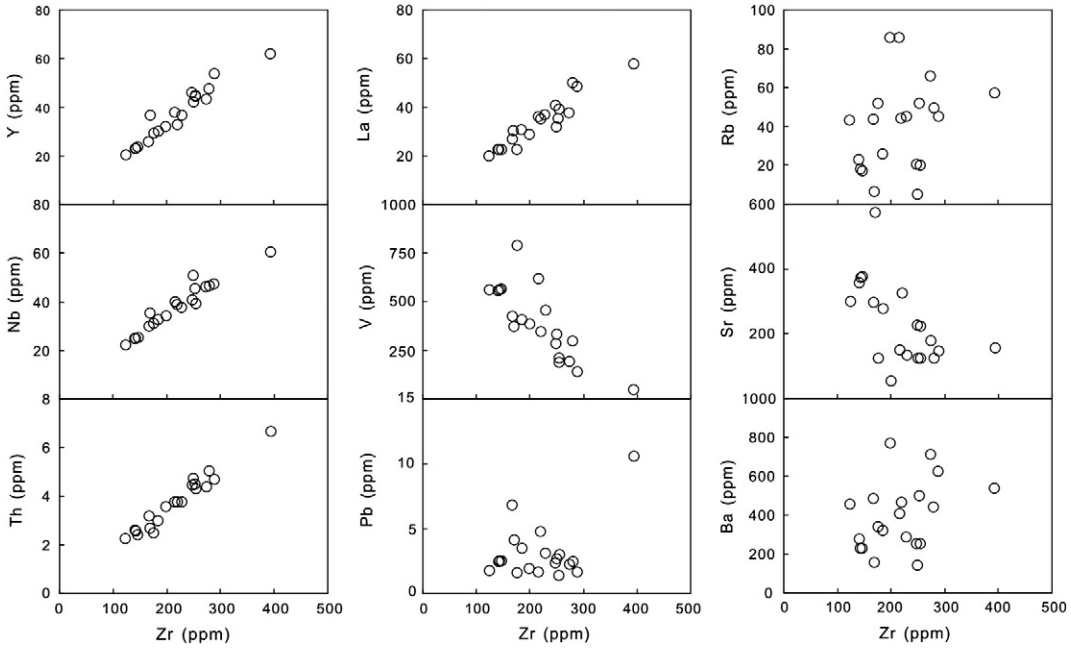

Fig. 8. Diagrams of Y, Nb, Th, La, V, Pb, Rb, Sr, and Ba vs. Zr to evaluate the mobility of these elements during alteration.

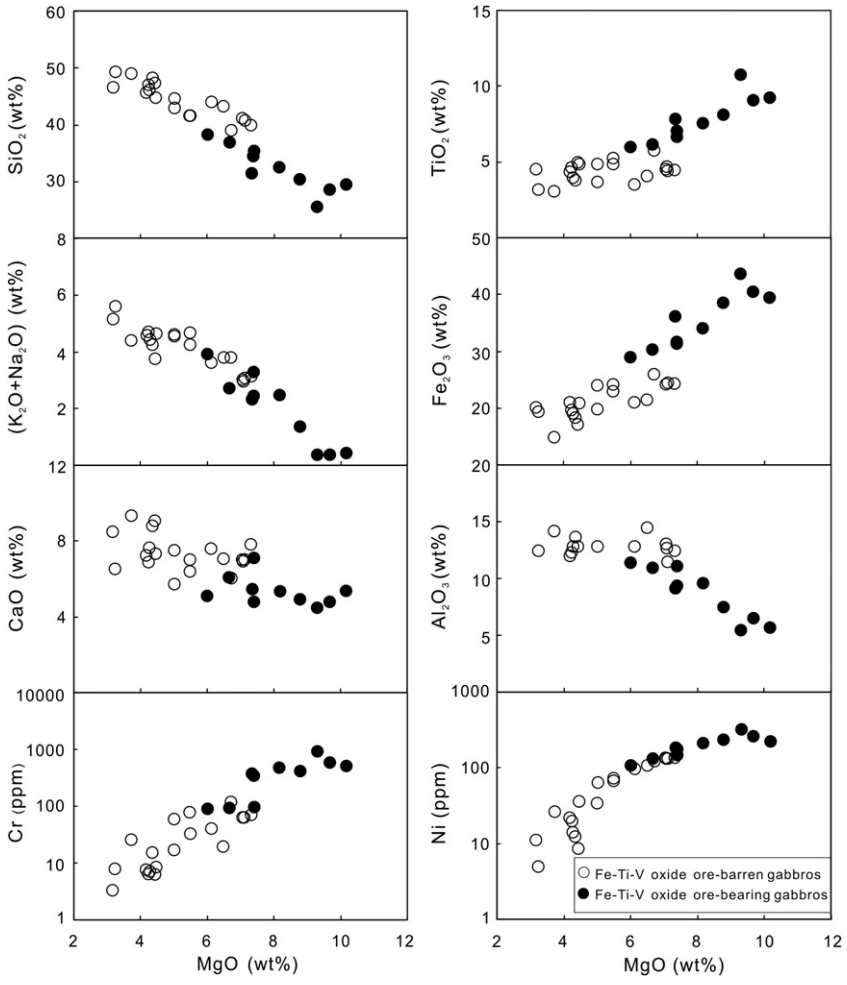

Fig. 9. Fenner diagrams for the Zhuqing gabbros.

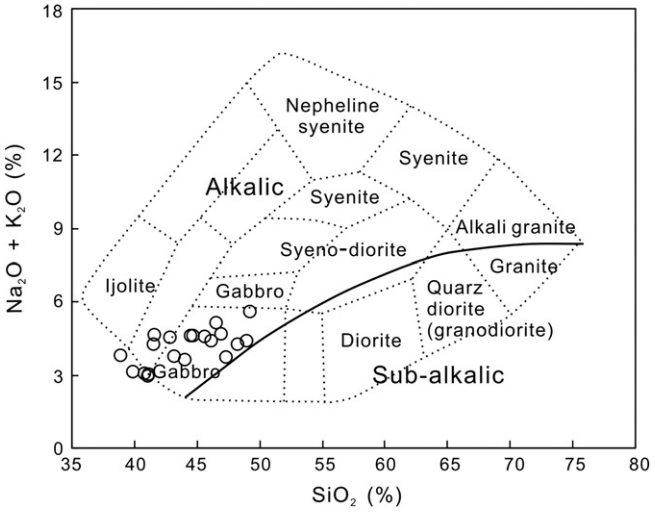

Fig. 10. Plots of SiO_2 vs. ($Na_2O + K_2O$) (Cox et al., 1979), for classification of the Fe–Ti–V oxide ore-barren rocks in the Zhuqing gabbros.

In the ore-barren gabbros, Fe_2O_3 and TiO_2 decrease with MgO contents (Fig. 9), likely reflecting fractional crystallization of Fe–Ti oxides (titanomagnetite and ilmenite). On the other hand, slight increases in CaO, Al_2O_3 and ($K_2O + Na_2O$) with decreasing MgO contents in the ore-barren rocks (Fig. 9) imply that plagioclase was not involved in fractional crystallization (e.g., Pik et al., 1998).

The Fe–Ti–V ore-bearing gabbros display higher Fe_2O_3 and TiO_2 contents than the ore-barren rocks, suggesting that they were controlled dominantly by accumulation of Fe–Ti oxides (Fig. 9). In addition, the positive correlations of Cr and Ni with MgO contents (Fig. 9) have also been mainly attributed to accumulation of Fe–Ti oxides, which is consistent with the compatible behavior of Cr and Ni in magnetite ($D_{Cr}^{Mt/liq} = 153$, Rollinson, 1993; $D_{Ni}^{Mt/liq} = 31–65$, Nielsen, 1992).

The ore-barren rocks are characterized by little evidence of depletion in Nb–Ta relative to the neighboring elements in the trace element multi-elament plot [$(Nb/La)_{PM} = 0.90–1.54$, $(Ta/La)_{PM} = 0.98–1.89$] (Fig. 11b), indicating that crustal contamination was not significant because continental crust is typically depleted in Nb and Ta (e.g., Rudnick and Fountain, 1995). It is noted, however, that there are positive correlations between $\varepsilon_{Nd}(T)$ values and Ta/La ratios (Fig. 12a) and between $\varepsilon_{Nd}(T)$ values and Th/La ratios (Fig. 12b), suggesting that the relative enrichment of La and slight depletion of Th and Ta in these rocks were likely due to minor crustal contamination (e.g., Paces and Bell, 1989).

In summary, fractional crystallization of Fe–Ti oxides appears to have played a major role in the compositional evolution of the Zhuqing rocks, whereas little crustal materials were involved in the magma evolutional process.

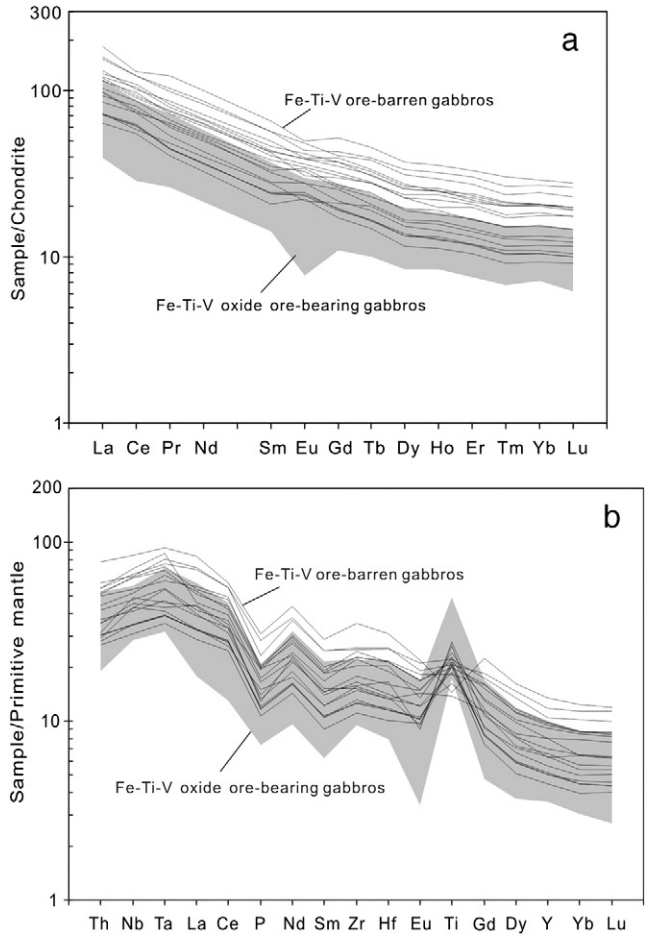

Fig. 11. a) Chondrite-normalized REE patterns of the Zhuqing gabbros, with normalizing values from Boynton (1984). b) Primitive mantle-normalized incompatible trace element spider diagram for the Zhuqing gabbros, with normalizing values from Sun and McDonough (1989).

5.2.2. Parental magma and mantle source

The parental magma composition of the Zhuqing intrusions is difficult to estimate, because: a) the cumulate rocks do not represent original liquid compositions (Wager and Brown., 1968); b) they do not have obvious chilled margins that can be used for estimating parental magma compositions; c) it is impossible to get the original mineral compositions due to significant alteration (Fig. 4b) to constrain the parent magma; and d) all the Zhuqing gabbros are quite rich in Fe and Ti but poor in Si with the oxide ore bodies having even higher Fe and Ti contents. In the ELIP, all the Fe–Ti oxide ore deposits appear to have formed from high-Ti magmas (Zhou et al., 2008). Therefore, the Zhuqing intrusions were likely crystallized from a relatively high Fe and high Ti magma.

Fractional crystallization of mineral phases such as olivine and/or clinopyroxene can result in Fe enrichment in the residual liquids (Thy et al., 2006; Toplis and Carroll, 1995). Intrusion of Fe-enriched and relatively Si-poor melts has been proposed to explain the upper part of the Skaergaard intrusion, Greenland (Brooks et al., 1991; Hunter and Sparks, 1987). As a result of extensive fractionation, magmas in the Skaergaard intrusion evolved into Fe-rich melts, which eventually became FeO saturated, and formed the Fe–Ti–V-oxide-rich rocks of the Triple Group (e.g., Wager and Brown, 1968). In the Bushveld Complex, a lengthy period of fractional crystallization of plagioclase resulted in residual magmas becoming enriched in Fe, Ti and V to form a denser and stagnant layer containing abundant discrete V-bearing titanomagnetite grains in the upper zone (Tegner et al., 2006). Zhou et al. (2005) suggested that the high-Fe liquids of the Panzhihua gabbroic intrusion were formed through fractional crystallization of olivine, clinopyroxene and plagioclase, and thus were highly evolved magmas. The Fe–Ti–V oxide-bearing ores and gabbroic rocks in the Zhuqing intrusions are relatively rich in Cu, resulting in high Cu/Ni ratios (average 3.2), a characteristic of high degrees of fractionation (e.g., Lesher and Keays, 2002). The depletion of Ni relative to Cu can be explained by fractionation of olivine, which preferentially concentrates Ni (Barnes et al., 1985). These features, together with very low MgO, Cr and Ni contents (Table 1), and LREE enrichment ($La_N = 39–185$) (Fig. 11a), are consistent with the parental magmas of the Zhuqing intrusions being highly evolved. Thus, the Fe–Ti-rich magma parental to the Zhuqing gabbros is likely to have been highly evolved and fractionationated.

Table 2
Sm–Nd isotopic compositions of the Zhuqing intrusions.

Sample	Sm (ppm)	Nd (ppm)	$^{147}Sm/^{144}Nd$	$^{143}Nd/^{144}Nd$	(2σ)	$(^{143}Nd/^{144}Nd)_I$	$\varepsilon_{Nd}(T)$
JQ1002	9.180	42.07	0.1320	0.511862	0.000004	0.510569	−2.79
JQ1005	7.294	34.14	0.1293	0.511795	0.000006	0.510529	−3.58
JQ1008	8.155	35.76	0.1380	0.512014	0.000004	0.510663	−0.97
JQ1010	7.349	35.21	0.1263	0.511815	0.000002	0.510579	−2.60
ZK0404	3.924	20.11	0.1180	0.511802	0.000006	0.510646	−1.29
ZK0406	8.176	39.76	0.1244	0.511829	0.000006	0.510611	−1.97
ZK0408	13.50	65.47	0.1248	0.511837	0.000004	0.510615	−1.89
ZK0101	4.640	21.76	0.1290	0.511828	0.000006	0.510565	−2.88
ZK0103	5.436	25.03	0.1314	0.511849	0.000006	0.510562	−2.93
ZK0105	6.157	29.94	0.1244	0.511833	0.000004	0.510614	−1.91
ZK2813	8.220	38.38	0.1296	0.511865	0.000004	0.510597	−2.26
ZK2821	4.055	19.57	0.1253	0.511850	0.000004	0.510623	−1.74
ZK2841	10.33	46.77	0.1337	0.511899	0.000004	0.510590	−2.38
ZK3601	7.900	37.42	0.1277	0.511828	0.000002	0.510577	−2.63
ZK3619	7.836	37.25	0.1273	0.511798	0.000004	0.510552	−3.14

Chondrite uniform reservoir (CHUR) values ($^{147}Sm/^{144}Nd = 0.1967$, $^{143}Nd/^{144}Nd = 0.512638$) are used for the calculation. $\lambda_{Sm} = 6.54 \times 10^{-12}$ year^{-1} (Lugmair and Harti, 1978). The $(^{143}Nd/^{144}Nd)_I$ and ε_{Nd} (T) were calculated using the age of 1490 Ma.

Toplis and Carroll (1995) demonstrated that primary mantle magmas need to undergo at least 60% crystal fractionation before magnetite appears on the liquidus. The presence of Fe–Ti oxide deposits in the upper zones of the Zhuqing gabbroic intrusions is consistent with a common observation that Fe–Ti oxide layers occur in the evolved upper parts of large layered intrusions around the world, such as the Bushveld Complex (Tegner et al., 2006), the Skaergaard intrusion (McBirney, 1996) and the Muskox intrusion (Irvine, 1988). This demonstrates that the Fe–Ti oxides may have formed late in the crystallization sequence. Therefore, late-stage fractional crystallization of titanomagnetite and ilmenite from an evolved and high Fe and Ti parental magma might have resulted in the formation of the Fe–Ti–V oxide deposits in the Zhuqing intrusions.

Their moderately sloping chondrite-normalized HREE patterns (Fig. 11a) and negative $\varepsilon_{Nd}(T)$ values indicate a derivation from a time-integrated, slightly enriched mantle source for the Zhuqing gabbros. The enriched signatures could have been inherited from either the sub-continental lithospheric mantle (SCLM) or an enriched deep asthenospheric mantle. The lack of Nb–Ta depletion and high-Ti nature of the parental magma suggests that the SCLM was not the reservoir that contributed to the trace element and Nd isotope inventory of the Zhuqing rocks. In general, low ratios of La/Yb in mafic rocks reflect a melting regime dominated by relatively large melt fractions and/or having spinel as the predominant residual phase, whereas high La/Yb ratios are indicative of smaller melt fractions and/or garnet control (Deniel, 1998; Xu et al., 2001). The fractionation of the HREE and high La/Yb ratios shown by the Zhuqing rocks suggest the presence of residual garnet during partial melting, a feature of melting at deep asthenospheric mantle sources. Meanwhile, the degree of partial melting to form the high-Ti basaltic magma for the Zhuqing intrusions is constrained by the high concentrations of incompatible elements of the rocks. The relatively high $(Sm/Yb)_{PM}$ ratios (2.0 to 2.5) of the Zhuqing rocks suggest small degrees of partial melting of a relatively deep mantle source. Therefore, the Zhuqing intrusions are interpreted as products of fractional crystallization from a parent magma generated by low degrees of partial melting of a slightly enriched asthenospheric mantle source.

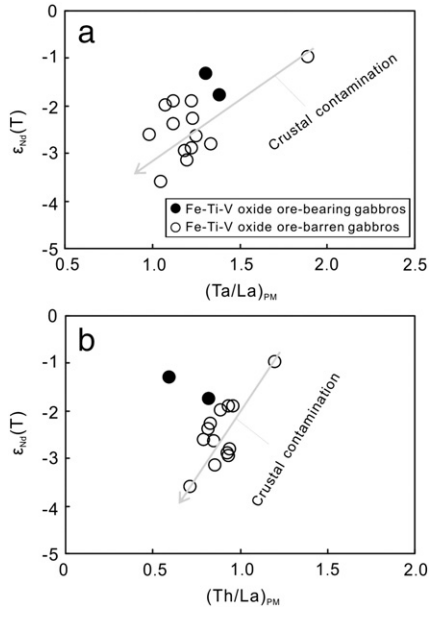

Fig. 12. Plots of (a) $\varepsilon_{Nd}(T)$ vs. $(Ta/La)_{PM}$, and (b) $\varepsilon_{Nd}(T)$ vs. $(Th/La)_{PM}$, for samples of the Zhuqing intrusions.

5.3. Tectonic implications

Magmatic Fe–Ti–V oxide ore deposits are typically hosted in mafic-ultramafic, plume-related layered intrusions or large igneous provinces (LIPs). For instance, the ca. 2.06 Ga Bushveld Complex in South Africa hosts magnetite layers in the upper zones (Tegner et al., 2006); the Coppermine River LIP in Canada hosts Fe–Ti–V oxide ore deposits in the ca. 1.27 Ga Muskox intrusion (Irvine, 1988; LeCheminant and Heaman, 1989); the ca. 260 Ma ELIP near the study region hosts the Panzhihua mine (1333 Mt ore reserves), the Baima mine (1497 Mt ore reserves) and the Hongge deposit (4572 Mt ore reserves) (e.g., Zhou et al., 2005, 2008); and the ca. 55 Ma North Atlantic LIP in East Greenland also host economic Fe–Ti–V oxide layers in the upper parts of the Skaergaard intrusion (Hirschmann et al., 1997; McBirney, 1996). The ca. 1.5 Ga Zhuqing intrusions contain Fe–Ti–V oxide ore deposits with over 100 Mt ore reserves in three intrusive bodies, and the rest of the Zhuqing intrusions also have Fe–Ti–V oxide mineralization potential. Such a potential plume/LIP connection is consistent with the early Mesoproterozoic intraplate, continental rift setting in the western Yangtze Block as the late Paleoproterozoic to early Mesoproterozoic strata in the region probably formed in an intra-continental rift basin (Zhao et al., 2010).

The ca 1.5 Ga age of the Zhuqing intrusions is consistent with widespread 1.6–1.3 Ga Mesoproterozoic post-orogenic and anorogenic magmatism that have been recognized in most Precambrian cratons worldwide. These include the 1.6 Ga Dalma magmatic rocks in northeast India (Roy et al., 2002), the 1.6–1.4 Ga anorthosite–monzonite–charnockite–rapakivi granite (AMCG) intrusive bodies in both North American and southern Baltica (Åhäll et al., 2000; Puura and Faloden,

1999), the 1.6–1.3 Ga Sn-bearing granite in the Amazonia Craton (Bettencourt et al., 1999), the 1.59 Ga tholeiitic dyke swarms in South American (Teixeira et al., 2012), the 1.5 Ga discontinuous granite–rhyolite terrane in eastern India (Deb, 2003), the 1.5 Ga mafic dykes in South American (Silveira et al., 2012), the 1.4 Ga Nova Guarita dyke swarm (Bispo-Santos et al., 2012) and Indiavaí mafic intrusive rocks (D'Agrella-Filho et al., 2012) in southwestern Amazonian, the 1.3 Ga Mackenzie dyke swarm in North American (Lecheminant and Heaman, 1989), the 1.38 Ga Mashak LIP in eastern Baltica (Puchkov et al., 2012), the 1.35 Ga diabase sills (Zhang et al., 2009) and 1.32 Ga A-type granite (Shi et al., 2012) in north China, the 1.32 Ga Galiwinku dyke swarm in Australia (Goldberg, 2010), the 1.3–1.2 Ga Gardar alkaline rock suite in southern Greenland (Macdonald and Uptonb, 1993), and the 1.26 Ga Satakunta–Ulvö Dyke Swarm in northern Baltica (Goldberg, 2010), among others.

The development of these global Mesoproterozoic anorogenic magmatism have been interpreted to be associated with the fragmentation of the Paleo- to Mesoproterozoic supercontinent Nuna that formed through continental collisions ca. 2.0–1.8 Ga (Evans and Mitchell, 2011; Hoffman, 1997; Zhang et al., 2012). The fragmentation of the supercontinent was proposed to have started about 1.6 Ga ago, associated with widespread continental rifting and anorogenic magmatism, and continued until its final break-up at about 1.2 Ga ago, marked by the emplacement of the 1.27 Ga Mackenzie and 1.24 Ga Sudbury mafic dyke swarms in North America (Evans and Mitchell, 2011; Rogers and Santosh, 2002; Zhang et al., 2012; Zhao et al., 2004). More recently, it was suggested that even the 1.84–1.75 Ga mafic dyke swarms and 1.75–1.68 Ga anorthosite–mangerite–alkali granite–rapakivi granite suites (AMGRS) in the North China Craton may have resulted from the fragmentation of the supercontinent Nuna (e.g., Hou et al., 2008a; Peng et al., 2006, 2008; Zhao et al., 2002b). These late Paleo- to Mesoproterozoic anorogenic magmatism associated with the break-up of the supercontinent Nuna have generally been linked to mantle plume activity (Evans and Mitchell, 2011; Hoffman, 1989; Hou et al., 2008a; Peng et al., 2008; Rogers and Santosh, 2002; Roy et al., 2002; Silveira et al., 2012; Teixeira et al., 2012; Zhao et al., 2002a, 2004) that can drive melts from different source regions, resulting in wide variations in the isotopic characteristics of magmatic rocks. The slightly enriched signature of the 1.5 Ga Zhuqing intrusions in this study, interpreted as being inherited from the asthenospheric mantle with little contribution from the SCLM or subducted slab (see Section 5.2), is also consistent with a possible mantle plume connection in their generation. Therefore, the Zhuqing intrusions were likely a part of global magmatic events related to activity of mantle plumes during the break-up of the supercontinent Nuna. If correct, it implies that the Yangtze Block may have been a component of the Paleo- to Mesoproterozoic supercontinent Nuna. However, the precise position and role of the Yangtze Block in the assembly and break-up of the supercontinent require further investigation.

6. Conclusions

We report results of the first detailed geochronological and geochemical analyses on newly discovered Mesoproterozoic gabbros in western Yangtze Block, South China. The following are our main findings:

(1) The crystallization age of the Zhuqing intrusions is ~1.5 Ga, as demonstrated by a weighted mean zircon $^{207}Pb/^{206}Pb$ age of 1494 ± 6 Ma, and mean baddeleyites $^{207}Pb/^{206}Pb$ ages of 1486 ± 3 Ma and 1490 ± 4 Ma, respectively.

(2) The Zhuqing gabbros were fractionally crystallized from a parental magma generated by melting of a slightly enriched asthenospheric mantle source in a continental rift environment with no obvious crustal contamination.

(3) The Yangtze Block was likely a fragment of the Paleo- to Mesoproterozoic supercontinent Nuna, and the 1.5 Ga Zhuqing gabbros are the first rocks reported from South China likely formed above a mantle plume that contributed to the break-up of the supercontinent Nuna.

Supplementary data to this article can be found online at http://dx.doi.org/10.1016/j.lithos.2013.02.004.

Acknowledgments

We appreciate Q.L. Li, Y. Liu, G.Q. Tang, and H. Tao for their assistances in SIMS dating, Y. Liu for major element analyses by XRF, J. Hu, G.P. Bao and Y. Huang for trace element analyses by ICP-MS, F. Xiao, and X.B. Li for Nd isotope analyses by TIMS. The paper has benefited from constructive comments of X.H. Li, X.C. Wang, H.L. Deng, two anonymous reviewers and chief editor A. Kerr. This work is jointly supported by 973 Program (2009CB421003), the Chinese Academy of Sciences (KZCX-YW-136-1), the NSFC (Grants 41273049, 41073043, and 40903022), and a Special Research Fund of the SKLOG, IGCAS. This is TIGeR publication No. 450 and contribution 293 from the ARC Center of Excellence for Core to Crust Fluid Systems (http://www.ccfs.mq.edu.au/).

References

Åhäll, K.I., Connelly, J.N., Brewer, T.S., 2000. Episodic rapakivi magmatism due to distal orogenesis?: correlation of 1.69–1.50 Ga orogenic and inboard "anorogenic" events in the Baltic shield. Geology 28, 823–826.
Barnes, S.-J., Naldrett, A.J., Gorton, M., 1985. The origin of the fractionation of platinum-group elements in terrestrial magmas. Chemical Geology 53, 303–323.
Bettencourt, J.S., Tosdal, R.M., Leite, W.B., Payolla, B.L., 1999. Mesoproterozoic rapakivi granites of the Rndônian tin province, southwestern border of the Amazon craton, Brazil. Reconnaissance U–Pb geochronology and regional implication. Precambrian Research 95, 41–67.
Bispo-Santos, F., D'Agrella-Filho, M.S., Trindade, R.I.F., Elming, S.-Å., Janikian, L., Vasconcelos, P.M., Perillo, B.M., Pacca, I.I.G., Silva, J.A., Barros, M.A.S., 2012. Tectonic implications of the 1419 Ma Nova Guarita mafic intrusives paleomagnetic pole (Amazonian Craton) on the longevity of Nuna. Precambrian Research 196–197, 1–22.
Boynton, W.V., 1984. Geochemistry of the rare earth elements: meteorite studies. In: Henderson, P. (Ed.), Rare Earth Element Geochemistry. Elsevier, pp. 63–114.
Brooks, C.K., Larsen, I.M., Nielsen, T.F.D., 1991. Importance of iron-rich tholeiitic magmas at divergent plate margins—a reappraisal. Geology 19, 269–272.
Buchan, K.L., Ernst, R.E., Hamilton, M.A., Mertanen, S., Pesonen, L.J., Elming, S.A., 2001. Rodinia: the evidence from integrated paleomagnetism and U–Pb geochronology. Precambrian Research 110, 9–32.
Chen, R.X., Zheng, Y.F., Xie, L.W., 2010. Metamorphic growth and recrystallization of zircon: distinction by simultaneous in-situ analyses of trace elements, U–Th–Pb and Lu–Hf isotopes in zircons from eclogite-facies rocks in the Sulu orogen. Lithos 114, 132–154.
Condie, K.C., 2002. Breakup of a Paleoproterozoic supercontinent. Gondwana Research 5, 41–43.
Cox, K.G., Bell, J.D., Pankhurst, R.J., 1979. The Interpretation of Igneous Rocks. Allen and Unwin, London, UK (450 pp.).
D'Agrella-Filho, M.S., Trindade, R.I.F., Elming, S.-A., Teixeira, W., Yokoyama, E., Tohver, E., Geraldes, M.C., Pacca, I.I.G., Barros, M.A.S., Ruiz, A.S., 2012. The 1420 Ma Indiavaí Mafic Intrusion (SW Amazonian Craton): paleomagnetic results and implications for the Columbia supercontinent. Gondwana Research 22, 956–973.
Dalziel, I.W.D., 1995. Earth before Pangea. Scientific American 272, 58–63.
Deb, S.P., 2003. Proterozoic felsic volcanism in the Pranhita–Godavari valley, India: its implication on the origin of the basin. Journal of Asian Earth Sciences 21, 623–631.
Deniel, C., 1998. Geochemical and isotopic (Sr, Nd, Pb) evidence for plume–lithosphere interactions in the genesis of Grande Comore magmas (Indian Ocean). Chemical Geology 144, 281–303.
Ernst, R.E., Wingate, M.T.D., Buchan, K.L., Li, Z.X., 2008. Global record of 1600–700 Ma Large Igneous Provinces (LIPs): implications for the reconstruction of the proposed Nuna (Columbia) and Rodinia supercontinents. Precambrian Research 160, 159–178.
Evans, D.A.D., Mitchell, R.N., 2011. Assembly and breakup of the core of Paleoproterozoic–Mesoproterozoic supercontinent Nuna. Geology 39, 443–446.
Gao, S., Yang, J., Zhou, L., Li, M., Hu, Z., Guo, J., Yuan, H., Gong, H., Xiao, G., Wei, J., 2011. Age and growth of the Archean Kongling terrain, South China, with emphasis on 3.3 Ga granitoid gneisses. American Journal of Science 311, 153–182.
Geng, Y., Yang, C., Du, L., Wang, X., Ren, L., Zhou, X., 2007. Chronology and tectonic environment of the Tianbaoshan formation: new evidence from zircon SHRIMP U–Pb age and geochemistry. Geological Review 53, 556–563 (in Chinese with English abstract).
Goldberg, A.S., 2010. Dyke swarms as indicators of major extensional events in the 1.9–1.2 Ga Columbia supercontinent. Journal of Geodynamics 50, 176–190.

Greentree, M.R., Li, Z.X., 2008. The oldest known rocks in south-western China: SHRIMP U–Pb magmatic crystallization age and detrital provenance analysis of the Paleoproterozoic Dahongshan Group. Journal of Asian Earth Sciences 33, 289–302.
Greentree, M.R., Li, Z.X., Li, X.H., Wu, H., 2006. Late Mesoproterozoic to earliest Neoproterozoic basin record of the Sibao orogenesis in western South China and relationship to the assembly of Rodinia. Precambrian Research 151, 79–100.
He, D.F., 2009. Petrological and geochemical characteristics of the Lala copper deposit in Sichuan Province. Unpublished PhD thesis, The Gradute School of the Chinese Academy of Sciences, China, 103 pp. (in Chinese with English abstract).
Hirschmann, M.M., Renneb, P.R., McBirneyc, A.R., 1997. $^{40}Ar/^{39}Ar$ dating of the Skaergaard intrusion. Earth and Planetary Science Letters 146, 645–658.
Hoffman, P.F., 1989. Speculations on Laurentia's first gigayear (2.0 to 1.0 Ga). Geology 17, 135–138.
Hoffman, P.F., 1991. Did the breakout of Laurentia turn Gondwanaland insideout? Science 252, 1409–1412.
Hoffman, P.F., 1997. Tectonic genealogy of North America. In: Van der Pluijm, B.A., Marshak, S. (Eds.), Earth Structure: an Introduction to Structural Geology and Tectonics. McGraw-Hill, New York, pp. 459–464.
Hoskin, P.W.O., Schaltegger, U., 2003. The composition of zircon and igneous and metamorphic petrogenesis. In: Hanchar, J.M., Hoskin, P.W.O. (Eds.), Zircon: Reviews in Mineralogy and Geochemistry, 53, pp. 27–62.
Hou, G., Li, J.H., Yang, M.H., Yao, W.H., Wang, C.C., Wang, Y.X., 2008a. Geochemical constraints on the tectonic environment of the Late Paleoproterozoic mafic dyke swarms in the North China Craton. Gondwana Research 13, 103–116.
Hou, G., Santosh, M., Qian, X., Lister, G.S., Li, J., 2008b. Configuration of the Late Paleoproterozoic supercontinent Columbia: insights from radiating mafic dyke swarms. Gondwana Research 14, 395–409.
Hunter, R.H., Sparks, R.S.J., 1987. The differentiation of the Skaergaard intrusion. Contributions to Mineralogy and Petrology 95, 451–461.
Irvine, T.N., 1988. Muskox intrusion, Northwest Territories. Geological environments of the platinum-group elements: Geological Survey of Canada Open File, 1440, pp. 25–39.
LeCheminant, A.N., Heaman, L.M., 1989. Mackenzie igneous events, Canada: middle Proterozoic hotspot magmatism associated with ocean opening. Earth and Planetary Science Letters 69, 169–191.
Lesher, C.M., Keays, R.R., 2002. Komatiite-associated Ni–Cu-(PGE) deposits. In: Cabri, L.J. (Ed.), The Geology, Geochemistry, Mineralogy, Mineral Beneficiation of the Platinum-Group Elements: Canadian Institute of Mining, Metallurgy and Petroleum, Special Volume, 54, pp. 579–618.
Li, Z.X., Evans, D.A.D., 2011. Late Neoproterozoic 40° intraplate rotation within Australia allows for a tighter-fitting and longer-lasting Rodinia. Geology 39, 39–42.
Li, Z.X., Zhang, L., Powell, C.McA., 1995. South China in Rodinia: part of the missing link between Australia–East Antarctica and Laurentia? Geology 23, 407–410.
Li, Z.X., Li, X.H., Zhou, H., Kinny, P.D., 2002. Grenvillian continental collision in South China: new SHRIMP U–Pb zircon results and implications for the configuration of Rodinia. Geology 30, 163–166.
Li, X.H., Li, Z.X., Sinclair, J.A., Li, W.X., Carter, G., 2006. Revisiting the "Yanbian Terrane": implications for Neoproterozoic tectonic evolution of the western Yangtze Block, South China. Precambrian Research 151, 14–30.
Li, Z.X., Wartho, J.A., Occhipinti, S., Zhang, C.L., Li, X.H., Wang, J., Bao, C.M., 2007. Early history of the eastern Sibao orogen (South China) during the assembly of Rodinia: new $^{40}Ar/^{39}Ar$ dating and U–Pb SHRIMP detrital zircon provenance constraints. Precambrian Research 159, 74–94.
Li, Z.X., Bogdanova, S.V., Collins, A.S., Davidson, A., De Waele, B., Ernst, R.E., Fitzsimons, I.C.W., Fuck, R.A., Gladkochub, D.P., Jacobs, J., Karlstrom, K.E., Lu, S., Natapovm, L.M., Pease, V., Pisarevsky, S.A., Thrane, K., Vernikovsky, V., 2008. Assembly, configuration, and break-up history of Rodinia: a synthesis. Precambrian Research 160, 179–210.
Li, X.H., Liu, Y., Li, Q.L., Guo, C.H., Chamberlain, K.R., 2009. Precise determination of Phanerozoic zircon Pb/Pb age by multi-collector SIMS without external standardization. Geochemistry, Geophysics, Geosystems 10, Q04010. http://dx.doi.org/10.1029/2009GC002400.
Li, Q.L., Li, X.H., Liu, Y., Tang, G.Q., Yang, J.H., Zhu, W.G., 2010. Precise U–Pb and Pb–Pb dating of Phanerozoic baddeleyite by SIMS with oxygen flooding technique. Journal of Analytical Spectrometry 25, 1107–1113.
Lugmair, G.W., Harti, K., 1978. Lunar initial $^{143}Nd/^{144}Nd$: differential evolution of the lunar crust and mantle. Earth and Planetary Science Letters 39, 349–357.
Macdonald, R., Uptonb, G.C., 1993. The Proterozoic Gardar rift zone, South Greenland: comparisons with the East African rift system. Geological Society, London Special Publications 76, 427–442.
McBirney, A.R., 1996. The Skaergaard intrusion. In: Cawthorn, R.G. (Ed.), Layered Intrusions. Elsevier, pp. 147–180.
Meert, J.G., 2002. Paleomagnetic evidence for a Paleo-Mesoproterozoic supercontinent Columbia. Gondwana Research 5, 207–216.
Meert, J.G., 2012. What's in a name? The Columbia (Paleopangaea/Columbia) supercontinent. Gondwana Research 21, 987–993.
Moores, E.M., 1991. Southwest U.S.–East Antarctic (SWEAT) connection: a hypothesis. Geology 19, 425–428.
Nielsen, R., 1992. BIGD. FOR: a fortran program to calculate trace-element partition coefficients for natural mafic and intermediate composition magmas. Computers and Geosciences 18, 773–788.
Paces, J.B., Bell, K., 1989. Non-depleted sub-continental mantle beneath the Superior Province of the Canadian Shield: Nd–Sr isotopic and trace element evidence from midcontinent rift basalts. Geochimica et Cosmochimica Acta 53, 2023–2035.
Peng, P., Zhai, M.G., Guo, J.H., 2006. 1.80–1.75 Ga mafic dyke swarms in the central North China craton: implications for a plume-related break-up event. In: Hanski, E., Mertanen, S., Ramö, T., Vuollo, J. (Eds.), Dyke Swarms—Time Markers of Crustal Evolution. Taylor & Francis Publisher.
Peng, P., Zhai, M.-G., Ernst, R., Guo, J.-H., Liu, F., Hu, B., 2008. A 1.78 Ga Large Igneous Province in the North China craton: the Xiong'er Volcanic Province and the North China dyke swarm. Lithos 101, 260–280.
Peng, M., Wu, Y.B., Wang, J., Jiao, W.F., Liu, X.C., Yang, S.H., 2009. Paleoproterozoic mafic dyke from Kongling terrain in The Yangtze Craton and its implication. Chinese Science Bulletin 54, 1098–1104.
Peng, M., Wu, Y.B., Gao, S., Zhang, H.F., Wang, J., Liu, X.C., Gong, H.J., Zhou, L., Hu, Z.C., Liu, Y.S., Yan, H.L., 2012. Geochemistry, zircon U–Pb age and Hf isotope compositions of Paleoproterozoic aluminous A-type granites from the Kongling terrain, Yangtze Block: constraints on petrogenesis and geologic implications. Gondwana Research 22, 140–151.
Pesonen, L.J., Elming, S.A., Mertanen, S., Pisarevsky, S., D'Agrella-Filho, M.S., Meert, J.G., Schmidt, P.W., Abrahamsen, N., Bylund, G., 2003. Paleomagnetic configuration of continents during the Proterozoic. Tectonophysics 375, 289–324.
Pik, R., Deniel, C., Coulon, C., Yirgu, G., Hofmann, C., Ayalew, D., 1998. The north western Ethiopian plateau flood basalts: classification and spatial distribution of magma types. Journal of Volcanology and Geothermal Research 81, 91–111.
Polat, A., Hofmann, A.W., Rosing, M.T., 2002. Boninite-like volcanic rocks in the 3.7–3.8 Ga Isua greenstone belt, West Greenland: geochemical evidence for intraoceanic subduction zone processes in the early Earth. Chemical Geology 184, 231–254.
Puchkov, V.N., Bogdanova, S.V., Ernst, R.E., Kozlov, V.I., Krasnobaev, A.A., Söderlund, U., Wingate, M.T.D., Postnikov, A.V., Sergeeva, N.D., 2012. The ca. 1380 Ma Mashak igneous event of the Southern Urals. Lithos. http://dx.doi.org/10.1016/j.lithos.2012.08.021.
Puura, V., Faloden, T., 1999. Rapakivi–granite–anorthosite magmatism: a way of thinning and stabilization of the Svecofennian crust, Baltic, Sea basin. Tectonophysics 305, 75–92.
Qi, L., Hu, J., Grégoire, D.C., 2000. Determination of trace elements in granites by inductively coupled plasma mass spectrometry. Talanta 51, 507–513.
Rodionov, N.V., Belyatsky, B.V., Antonov, A.V., Kapitonov, I.N., Sergeev, S.A., 2012. Comparative in-situ U–Th–Pb geochronology and trace element composition of baddeleyite and low-U zircon from carbonatites of the Palaeozoic Kovdor alkaline–ultramafic complex, Kola Peninsula, Russia. Gondwana Research 2012, 728–744.
Rogers, J.J.W., 1996. A history of continents in the past three billion years. Journal of Geology 104, 91–107.
Rogers, J.J.W., 2012. Did natural fission of ^{235}U in the earth lead to formation of the supercontinent Columbia? Geoscience Frontiers 3, 369–374.
Rogers, J.J.W., Santosh, M., 2002. Configuration of Columbia, a Mesoproterozoic supercontinent. Gondwana Research 5, 5–22.
Rogers, J.J.W., Santosh, M., 2009. Tectonics and surface effects of the supercontinent Columbia. Gondwana Research 15, 373–380.
Rollinson, H., 1993. Using geochemical data: evaluation, presentation, interpretation. Longman Scientific & Technical. (108 pp.).
Roy, A., Sarkar, A., Jeyakumar, S., Aggrawal, S.K., Ebihara, M., 2002. Mid-Proterozoic plume related thermal event in eastern Indian craton: evidence from trace elements, REE geochemistry and Sr–Nd isotope systematics of basic-ultrabasic intrusives from Dalma volcanic belt. Gondwana Research 5, 133–146.
Rudnick, R.L., Fountain, D.M., 1995. Nature and composition of the continental crust: a lower crustal perspective. Reviews of Geophysics 33, 267–309.
Shi, Y.R., Liu, D.Y., Kröner, A., Jian, P., Miao, L.C., Zhang, F.Q., 2012. Ca. 1318 Ma A-type granite on the northern margin of the North China Craton: implications for intraplate extension of the Columbia supercontinent. Lithos 148, 1–9.
Silveira, E.M., Söderlund, U., Oliveira, E.P., Ernst, R.E., Menezes Leal, A.B., 2012. First precise U–Pb baddeleyite ages of 1500 Ma mafic dykes from the São Francisco Craton, Brazil, and tectonic implications. Lithos. http://dx.doi.org/10.1016/j.lithos.2012.06.004.
Sun, S.S., McDonough, W.F., 1989. Chemical and isotopic systematics of oceanic basalts: implications for mantle composition and processes. In: Saunders, A.D., Norry, M.J. (Eds.), Magmatism in the Ocean Basins: Geological Society, London Special Publications, 42, pp. 313–345.
Sun, M., Chen, N., Zhao, G., Wilde, S.A., Ye, K., Guo, J., Chen, Y., Yuan, C., 2008. U–Pb Zircon and Sm–Nd isotopic study of the Huangtuling granulite, Dabie–Sulu belt, China: implication for the Paleoproterozoic tectonic history of the Yangtze Craton. American Journal of Science 308, 469–483.
Sun, W.H., Zhou, M.F., Gao, J.F., Yang, Y.H., Zhao, X.F., Zhao, J.H., 2009a. Detrital zircon U–Pb geochronological and Lu–Hf isotopic constraints on the Precambrian magmatic and crustal evolution of the western Yangtze block, SW China. Precambrian Research 172, 99–126.
Sun, Z.M., Yin, F.G., Guan, J.L., Liu, J.H., Li, J.M., Geng, Y.R., Wang, L.Q., 2009b. SHRIMP U–Pb dating and its stratigraphic significance of tuff zircons from Heishan formation of Kunyang Group, Dongchuan area, Yunnan Province, China. Geological Bulletin of China 28, 896–900 (in Chinese with English abstract).
Tegner, C., Cawthorn, R.G., Kruger, F.J., 2006. Cyclicity in the main and upper zones of the Bushveld Complex, South Africa: crystallization from a zoned magma sheet. Journal of Petrology 47, 2257–2279.
Teixeira, W., DAgrella-Filho, M.S., Ernst, R.E., Hamilton, M.A., Girardi, V.A.V., Mazzucchelli, M., Bettencourt, J.S., 2012. U–Pb (ID-TIMS) baddeleyite ages and paleomagnetism of 1.79 and 1.59 Ga tholeiitic dyke swarms, and position of the Rio de la Plata Craton within the Columbia supercontinent. Lithos. http://dx.doi.org/10.1016/j.lithos.2012.09.006.
Thy, P., Lesher, C.E., Nielsen, T.F.D., Brooks, C.K., 2006. Experimental constraints on the Skaergaard liquid line of descent. Lithos 92, 154–180.
Toplis, M.J., Carroll, M.R., 1995. An experimental study of the influence of oxygen fugacity on Fe–Ti oxide stability, phase relations, and mineral-melt equilibria in ferro-basaltic systems. Journal of Petrology 36, 1137–1170.

Wager, L.R., Brown, G.M., 1968. Layered Igneous Rocks. Oliver and Boyd, Edinburgh and London (588 pp.).
Wang, L.J., Griffin, W.L., Yu, J.H., O'Reilly, S.Y., 2012. U–Pb and Lu–Hf isotopes in detrital zircon from Neoproterozoic sedimentary rocks in the northern Yangtze Block: implications for Precambrian crustal evolution. Gondwana Research. http://dx.doi.org/10.1016/j.gr.2012.04.013.
Wingate, M.T.D., Compston, W., 2000. Crystal orientation effects during ion microprobe U–Pb analysis of baddeleyite. Chemical Geology 168, 75–97.
Wood, D.A., Joron, J.L., Treuil, M., 1979. A re-appraisal of the use of trace elements to classify and discriminate between magma series erupted in different tectonic settings. Earth and Planetary Science Letters 45, 326–336.
Wu, Y.B., Zheng, Y.F., Gao, S., Jiao, W.F., Liu, Y.S., 2008. Zircon U–Pb age and trace element evidence for Paleoproterozoic granulite-facies metamorphism and Archean crustal rocks in the Dabie Orogen. Lithos 101, 308–322.
Xiong, Q., Zheng, J.P., Yu, C.M., Su, Y.P., Tang, H.Y., Zhang, Z.H., 2009. Zircon U–Pb age and Hf isotope of Quanyishang A-type granite in Yichang: signification for the Yangtze continental cratonization in Paleoproterozoic. Chinese Science Bulletin 54, 436–446.
Xu, Y.G., Chung, S.L., Jahn, B.M., Wu, G.Y., 2001. Petrologic and geochemical constraints on the petrogenesis of Permian–Triassic Emeishan flood basalts in southwestern China. Lithos 58, 145–168.
Yao, J., Shu, L., Santosh, M., 2011. Detrital zircon U–Pb geochronology, Hf-isotopes and geochemistry — new clues for the Precambrian crustal evolution of Cathaysia Block, South China. Gondwana Research 20, 553–567.
Zhang, S.B., Zheng, Y.F., Wu, Y.B., Zhao, Z.F., Gao, S., Wu, F.Y., 2006a. Zircon isotope evidence for ≥3.5 Ga continental crust in the Yangtze craton of China. Precambrian Research 146, 16–34.
Zhang, S.B., Zheng, Y.F., Wu, Y.B., Zhao, Z.F., Gao, S., Wu, F.Y., 2006b. Zircon U–Pb age and Hf–O isotope evidence for Paleoproterozoic metamorphic event in South China. Precambrian Research 151, 265–288.
Zhang, C.H., Gao, L.Z., Wu, Z.J., Shi, X.Y., Yan, Q.R., Li, D.J., 2007. SHRIMP U–Pb zircon age of tuff from the Kunyang group in central Yunnan: evidence for Grenvillian orogeny in south China. Chinese Science Bulletin 52, 1517–1525.
Zhang, S.H., Zhao, Y., Yang, Z.Y., He, Z.F., Wu, H., 2009. The 1.35 Ga diabase sills from the northern North China Craton: implications for breakup of the Columbia (Nuna) supercontinent. Earth and Planetary Science Letters 288, 588–600.
Zhang, S., Li, Z.X., Evans, D.A.D., Wu, H., Li, H., 2012. Pre-Rodinia supercontinent Nuna shaping up: a global synthesis with new paleomagnetic results from North China. Earth and Planetary Science Letters 353-354, 145–155.
Zhao, X.F., Zhou, M.F., 2011. Fe–Cu deposits in the Kangdian region, SW China: a Proterozoic IOCG (iron–oxide–copper–gold) metallogenic province. Mineralium Deposita 46, 731–747.
Zhao, G.C., Cawood, P.A., Wilde, S.A., Sun, M., 2002a. Review of global 2.1–1.8 Ga orogens: implications for a pre-Rodinia supercontinent. Earth-Science Reviews 59, 125–162.
Zhao, T.P., Zhou, M.F., Zhai, M.G., Xia, B., 2002b. Paleoproterozoic rift-related volcanism of the Xiong'er group, North China craton: implications for the breakup of Columbia. International Geology Review 44, 336–351.
Zhao, G.C., Sun, M., Wilde, S.A., Li, S.Z., 2004. A Paleo-Mesoproterozoic supercontinent: assembly, growth and breakup. Earth-Science Reviews 67, 91–123.
Zhao, X.F., Zhou, M.F., Li, J.W., Sun, M., Gao, J.F., Sun, W.H., Yang, J.H., 2010. Late Paleoproterozoic to early Mesoproterozoic Dongchuan Group in Yunnan, SW China: implications for tectonic evolution of the Yangtze Block. Precambrian Research 182, 57–69.
Zheng, J.P., Griffin, W.L., O'Reilly, S.Y., Zhang, M., Pearson, N., Pan, Y., 2006. Widespread Archean basement beneath the Yangtze Craton. Geology 34, 417–420.
Zhou, M.F., Robinson, P.T., Lesher, C.M., Keays, R.R., Zhang, C.J., Malpas, J., 2005. Geochemistry, petrogenesis and metallogenesis of the Panzhihua gabbroic layered intrusion and associated Fe–Ti–V oxide deposits, Sichuan province, SW China. Journal of Petrology 46, 2253–2280.
Zhou, M.F., Arndt, N.T., Malpas, J., Wang, C.Y., Kennedy, A., 2008. Two magma series and associated ore deposit types in the Permian Emeishan large igneous province, SW China. Lithos 103, 352–368.